HHS Public Access

Author manuscript

Histochem Cell Biol. Author manuscript; available in PMC 2024 August 18.

Published in final edited form as:

Histochem Cell Biol. 2024 July ; 162(1-2): 161–183. doi:10.1007/s00418-024-02297-7.

Crossing boundaries of light microscopy resolution discerns novel assemblies in the nucleolus

Carl C. Correll[1], **Udo Rudloff**[2], **Jeremy D. Schmit**[3], **David A. Ball**[4], **Tatiana S. Karpova**[4], **Eric Balzer**[5], **Miroslav Dundr**[2,6]

[1]Center for Proteomics and Molecular Therapeutics and Biochemistry and Molecular Biology, Chicago Medical School, Rosalind Franklin University of Medicine & Science, North Chicago, IL 60064, USA

[2]Rare Tumor Initiative, Pediatric Oncology Branch, Center for Cancer Research, National Cancer Institute, National Institutes of Health, Bethesda, MD 20892, USA

[3]Department of Physics, Kansas State University, Manhattan, KS 66506, USA

[4]Laboratory of Receptor Biology and Gene Expression, National Cancer Institute, National Institutes of Health, Bethesda, MD 20892, USA

[5]Nikon Instruments Inc., Melville, NY 11747, USA

[6]Center for Cancer Cell Biology, Chicago Medical School, Rosalind Franklin University of Medicine & Science, North Chicago, IL 60064, USA

Abstract

The nucleolus is the largest membraneless organelle and nuclear body in mammalian cells. It is primarily involved in the biogenesis of ribosomes, essential macromolecular machines responsible for synthesizing all proteins required by the cell. The assembly of ribosomes is evolutionarily conserved and accounts for the most energy-consuming cellular process needed for cell growth, proliferation, and homeostasis. Despite the significance of this process, the substructural mechanistic principles of the nucleolar function in preribosome biogenesis have only recently begun to emerge. Here, we provide a new perspective using advanced super-resolution microscopy and single-molecule MINFLUX nanoscopy on the mechanistic principles governing ribosomal RNA-seeded nucleolar formation and the resulting tripartite suborganization of the nucleolus driven, in part, by liquid–liquid phase separation. With recent advances in the cryogenic electron microscopy (cryoEM) structural analysis of ribosome biogenesis intermediates, we highlight the current understanding of the step-wise assembly of preribosomal subunits in the nucleolus. Finally, we address how novel anticancer drug candidates target early steps in ribosome biogenesis to exploit these essential dependencies for growth arrest and tumor control.

✉Miroslav Dundr, mirek.dundr@rosalindfranklin.edu.

Author contributions M.D., C.C., U.R., and J.S. wrote the main text. D.B. and T.K. wrote special sections of the manuscript, and M.D. prepared Figs. 1, 2, 3, 4, and 6. D.B. and T.K. prepared Fig. 5, and C.C. prepared Figs. 7 and 8. U.R. prepared Fig. 9 and the table. E.B. helped with Figs. 2, 3, and 6. All authors reviewed the manuscript.

Conflict of interests The authors declare no competing interests.

Keywords

Cancer; Nucleolus; Nucleolar subcompartmentalization; Phase separation; Pre-rRNA processing; rDNA genes

Introduction

Within this primary data overview, we explore the impact of recent microscopic advances that approach nanometer-scale molecular resolution and cryogenic electron microscopy (cryoEM) structures on our understanding of ribosome biogenesis. With the newly developed microscopy approaches, we can visualize single large macromolecular assemblies in the nucleolus, such as RNA polymerase I (pol I). This dedicated transcription machinery was initially characterized by transmission electron microscopy. Miller spreads of nucleolar chromatin showed transcription of ribosomal RNA (rDNA) genes by RNA pol I as compacted Christmas trees like structures with the small subunit (SSU) processome, required for the biogenesis of the 18S rRNA, appearing as terminal knobs on the 5′ end of nascent pre-rRNAs. Advances in determining cryoEM structures have more recently added a detailed roadmap of many processing and assembly intermediates in the biogenesis of both the small and large subunits (SSU and LSU), first from yeast and, more recently, from human sources. Herein, we will discuss the remaining gaps needed to link the atomic details of cryoEM microscopy used in structural biology with the emerging super-resolution and nanoresolution of light microscopy applied to cell biology.

Functional architecture of the nucleolus

The nucleolus is the primary site of rRNA synthesis, processing, and initial assembly steps of small and large preribosomal subunits. Among a plethora of diverse nuclear structures (Sawyer et al. 2019; Hirose et al. 2023), the nucleolus is the most prominent compartment, accounting for 20–25% of the total nuclear volume. Attesting to the nucleolus as a central hub regulating cellular biology, dynamic changes in the nucleolar size and fusion of nucleoli are associated with age, longevity, cancer, and different cellular conditions, including stress and viral infections (Miyake and McDermott 2023). When the cells exponentially proliferate, nucleoli size increases along with the number of newly synthesized proteins, and, conversely, size decreases when they are quiescent. Thus, larger nucleolar size and number have been used as prognostic biomarkers of malignancy (Penzo et al. 2019). Similar to other nuclear structures, the nucleolus is physically separated from the surrounding nucleoplasm without a defining membrane, which is thought to facilitate the dynamic exchange of components between the nucleolus and nucleoplasm. Despite its prominent microscopic visibility and well-defined proteome and RNA content, the mechanistic principles of orchestrating its nucleation, substructural maintenance, and functional suborganization remain poorly understood. In addition to its primary role in ribosome biogenesis, the nucleolus facilitates diverse cellular processes or pathways, such as control of cell cycle progression, aging, responses to cellular stress, DNA damage, mRNA export, and protein degradation (Boulon et al. 2010).

Transcription of ribosomal rDNA genes, which are arranged in tandem arrays, represents most of the transcriptional activity in eukaryotic cells, thereby comprising one of the most energy-consuming process linked to cell growth, ribosome biogenesis. Genome-wide sequencing analysis and genetic studies suggest that rDNA arrays have noteworthy variation in the number of copies across species (Parks et al. 2018). These rDNA genes occur as tandem repeats, ranging from 45 kb (~1 rDNA repeat) to 6 Mb (~140 repeats). They are organized as the nucleolus organizer regions (NORs) on the short arms of the acrocentric (with centromere located near the end of the chromosome) chromosomes 13, 14, 15, 21 and 22 in humans, and chromosomes 12, 15, 16, 18, and 19 in mouse (van Sluis et al. 2019). The precise organization and exact number of repeats are species, cell type, and age-dependent (Parks et al. 2018). Previously, the rRNA genes are believed to be highly conserved among species, apart from the ribosomal DNA intergenic spacers, which mainly contain repetitive and transposable elements, and contain transcription sites for regulatory RNAs involved in nucleolar integrity and connection between RNA pol I and II transcription. However, increasing evidence suggests that not all rRNA genes are identical and instead exist in several variants. Recent telomere-to-telomere (T2T) sequencing was used to determine complete gapless assemblies of the highly repetitive rDNA in human cells (Nurk et al. 2022). Within a cell, the 45 kb rDNA repeats are nearly but not completely identical. The length of these arrays varies between individuals, with an average of 315 rDNA copies and a standard deviation of 104 copies (Nurk et al. 2022).

Eukaryotic ribosome biogenesis requires the three major RNA polymerases: pol I, pol II and pol III. Human RNA pol I transcribes the polycistronic 47S pre-rRNA transcript (13.3 kb), which houses the 18S, 5.8S, and 28S rRNAs, with an elongation rate of ~95 nt/s (Dundr et al. 2002). These three rRNAs are flanked by external transcribed spacers (5′ETS and 3′ETS) and separated by internal transcribed spacers (ITS1 and ITS2). These spacer elements are essential for rRNA folding and assembly and are removed by irreversible cleavage events (Fig. 1b). RNA pol II transcribes ~80 ribosomal proteins (RPs) and about 200 trans-acting factors, which are needed to chaperone rRNA folding and RNP assembly, among other roles. The 40S small subunit forms with 33 RPs assembling with 18S rRNA, and the 60S large ribosomal subunit assembles with 47 RPs, 28S rRNA, 5S rRNA, and 5.8S rRNA. Each mRNA transcript encoding RPs or trans acting factors are first exported to the cytoplasm for translation and folding. Then, these proteins are imported back into the nucleus and eventually into the nucleolus where they will either assemble to form preribosomes as RPs or aid in their folding and assembly processes as trans-acting factors. RNA pol II also transcribes the snoRNAs predominantly from introns that guide central post-transcriptional rRNA chemical modifications, such as methylation and pseudouridylation, that chaperone folding and assembly (Kufel and Grzechnik 2019). RNA pol II also transcribes the most abundant snoRNA, U3 snoRNA (SNORD3A), from an independent gene, which assembles into a C/D box snoRNP, and plays a critical role in 18S rRNA folding and assembly (see below and Fig. 8). Also transcribed are several post-translational rRNA-modifying enzymes (Sloan et al. 2017). The fourth rRNA is 5S and is transcribed by RNA pol III, which is coregulated with RNA pol I to ensure equimolar production of each of the four mature rRNAs (Correll et al. 2019).

Why are there many rDNA genes?

During the 24 h that it takes for a typical rapidly proliferating human cell to divide up to 10 million functioning ribosomes must be made. Thus, an equal number of 47S pre-rRNA transcripts must be made within this time period. Each human RNA pol I transcribes one 47S transcript approximately every 140 s (Dundr et al. 2002) to produce, without possible transcription bursts (Fu et al. 2023), a little more than 600 transcripts in 24 h. The rate of RNA pol I transcription (Azouzi et al. 2021) cannot increase without loss of fidelity, so the evolutionary solution to satisfy cellular demand is parallel transcription. Each actively transcribing rDNA gene has up to 200 engaged RNA pol I holoenzymes that are simultaneously transcribing the primary 47S pre-rRNA. Similar to protein translation on polysomes, this parallel process increases throughput without sacrificing fidelity. This 200-fold parallel production produces over 120 thousand transcripts in 24 h, which, alas, is still insufficient. To overcome this shortfall, all eukaryotic genomes contain from 100 to 1000 s copies of the rDNA genes (Nelson et al. 2019). As mentioned, human diploid cells have about 400 rDNA genes, and it is estimated that about 200 or more of the rDNA genes are actively transcribing at any time in metabolically active cells (Srivastava et al. 2016). This final 200-fold amplification brings us up to 24 million 47S transcripts in 24 h, which is now sufficient to sustain rapid cell proliferation.

Ribosomal genes—“not all rDNA genes are created equal” and instead exist in several variants

As stated above, a typical diploid human genome contains an average of 400 copies of 45 kb rDNA unit with individual genetic polymorphism (Nurk et al. 2022). However, in metabolically active cells, not all rDNA genes are competent for transcription. Based on transcriptional activity and chromatin status, ribosomal genes are active, silenced, or constitutively inactive (Kresoja-Rakic and Santoro 2019). It is estimated that the epigenetic processes, including DNA methylation and histone post-translational modifications, silence about half of the rDNA genes (Srivastava et al. 2016). Active rDNA genes are transcribed by RNA pol I and associated with the essential transcription upstream binding factor (UBF), which replaces nucleosomes in coding regions by creating a nucleosome-like structure on rDNA (Gagnon-Kugler et al. 2009). By contrast, constitutively inactive genes are not transcriptionally active and do not interact with UBF. This chromatin is compacted with nucleosomes enriched in H3K9me3, which is a repressive histone mark, as in the case of silent rRNA genes.

To expand on these initial studies and to characterize the presence and distribution of active and inactive human rDNA genes within the nucleolus in better detail, we visualized rDNA gene repeats by 3D DNA FISH using multicolor super-resolution SIM imaging. To mark active rDNA transcription, we codetected DNA FISH signals with the largest subunit of RNA pol I RPA194 and NOLC1 (Nopp140), a phosphoprotein chaperone linking transcription with pre-rRNA processing (Fig. 1c, d). Our results revealed that the active rDNA genes marked by associated signals of RPA194 and NOLC1 are arranged inside the nucleolus in relaxed linear rDNA arrays filling most of the nucleolar interior. In

contrast, silenced rDNA genes (with absent RPA194 and NOLC1 signals) are present in smaller cumulative blocks in several distinct spatially segregated intranucleolar locations. Notably, inactive rDNA genes are predominantly localized in significantly larger blocks of heterochromatin localized at the periphery of the nucleolus, which is visualized by nucleophosmin/B23 (NPM1), a chaperone involved in preribosomal subunit assembly in the outer granular component (Fig. 1c, d). Our imaging indicates that active and transcriptionally silenced rDNA genes in the nucleolar interior are spatially segregated. Inactive rDNA genes are heavily compacted into distinct heterochromatin blocks that are nonrandomly positioned at the nucleolar periphery. Our finding of rDNA heterochromatin nonrandomly enriched at the periphery of the nucleolus supports the role of this region as a hub for the spatial organization of non-nucleolar heterochromatin domains (called Nucleolus-associated domains). These domains contain transcriptionally inactive genes across the genome and are thought to mediate genomic stability and regulate gene expression (Lindström et al 2018; Bizhanova et al. 2021). Interestingly, in humans, a 5S rDNA gene array containing 50 to 300 repeats on the q arm of chromosome 1 is also preferentially localized at the nucleolar periphery and interacts with inactive rDNA genes (Lemos et al. 2018).

How is step-wise preribosome biogenesis reflected in the subnucleolar architecture?

The step-wise process of biogenesis of pre-ribosomal subunits is reflected in the three-layered structures in the mature nucleolus: (1) multiple centrally-located fibrillar centers (FC), (2) each surrounded by the “ring-like” dense fibrillar component (DFC), and (3) peripherally-positioned continuous granular component (GC) (Fig. 1a). However, a high degree of morphological heterogeneity exists across nucleoli of different lineages of eukaryotic cells, from yeasts to mammals. Interestingly, yeast and other lower eukaryotes lack FCs, which might be linked to the closed nuclear division they usually undergo without the nuclear envelope breakdown (Thiry and Lafontaine 2005).

What are the key structural and functional characteristics of the three nucleolar subcompartments?

Fibrillar centers

The FC serves as the rRNA gene transcription site. The rDNA gene arrays located at NORs of five acrocentric chromosomes are anchored in the centrally positioned FCs, which appear as roundish structures of sizes ranging from 50 nm to, surprisingly, 1 μm (Fig. 3a). Transcriptionally active rDNA genes are located in the FC/DFC border region, with active rDNA genes forming loop complex structures. This loop formation facilitates efficient switching from termination to reinitiation of transcription by juxtaposing the promoter and terminator sequences (Denissov et al. 2011). This is consistent with the structural role of the architectural transcription factor UBF, which binds to active genes and clusters of transcriptionally inactive rDNA genes. As RNA pol I initiates transcription, the resulting nascent pre-rRNA immediately undergoes a complex series of association and dissociation of various trans-acting factors, which are tightly coupled to rRNA synthesis and processing.

Dense fibrillar component

The DFC contains newly synthesized pre-rRNAs. Since the human 47S primary transcript precursors are clearly detectable by northern blotting (Dundr and Olson 1998; Sirri et al. 2016), the levels of cotranscriptionally processed pre-rRNAs likely vary between individual rDNA gene loci. Released pre-rRNAs undergo in DFC a series of assembly, processing, modification, and folding steps. It has been proposed that the DFC signature protein, 2′-O-methyltransferase fibrillarin, forms a spherical cluster network that assembles into DFC surrounding the FC (Yao et al. 2019). Thus, the DFC consists of rRNA newly bound to RPs and trans-acting proteins, while the GC contains RNA bound to RPs and different trans-acting factors that are assembled into immature ribosomes.

Granular component

The nascent preribosomal particles move outwardly to become the granular components, where the assembly steps of preribosomal particles with RPs and RNA pol III-synthesized 5S rRNA occur. Additionally, some rRNA base modifications by snoRNPs and protein-based enzymes occur in the GC (Vanden Broeck et al. 2023). Upon exiting the GC, preassembled ribosome particles continue their vectorial path through the nucleoplasm, where they undergo additional assembly steps for eventual export to the cytoplasm for final assembly into fully functional ribosomes.

Importantly, the composition and the substructural definition of these subcompartments are incompletely defined on initial fixed transmission electron microscopy images. These definitions harbor an inherent, significant degree of heterogeneity due to the dynamic redistribution of assembly factors that vary with the status of preribosomal subunit production (Tartakoff et al. 2022). Moreover, the ability to locate the CryoEM structures is limited to individual subcompartments of the nucleolus, the nucleoplasm, or the cytoplasm, as a spatially unbiased substructural localization within the nucleolar architecture (such as DFC or GC) is currently not possible.

A critical question is how these three canonical nucleolar subcompartments are structurally, topologically, and functionally defined during ribosome biogenesis. Historically, electron transmission microscopy showed that the nucleolus was initially distinguished as a tripartite structure with higher electron density than the surrounding nucleoplasm (Olson and Dundr 2005; Pederson 2011). This technique revealed the pale-staining roundish FCs, surrounded by darkly stained DFCs with a high density of fibrils, indicating the presence of RNA. Both structures are encapsulated by an outer GC composed of granules of 15–20 nm in diameter (Fig. 1a). With the progressive development of fluorescence microscopy techniques, these subcompartments started to be identified using specific antibodies against marker proteins, RNA FISH probes, and, later, with expression of GFP-tagged marker proteins. Recent super-resolution microscopy studies estimate that a human cell’s nucleoli presents as either a single prominent nucleolus or several smaller nucleoli, which contain a total of several dozen small FC/DFC units that are assembled around the transcriptionally active rDNA gene tandem repeats. It has been further estimated that each FC/DFC unit contains one to three transcriptionally active rDNA genes situated at the FC/DFC boundary (Yao et al. 2019; Maiser et al. 2020). However, these estimates need more detailed 3D spatial analysis.

Moreover, the structural definition of these subcompartments still lacks detailed functional characterization.

Functional characterization of FC/DFC units

To further probe the underlying structural suborganization and topological arrangement of FC/DFC modules within the metabolically active nucleolus, we selected as established cell models the aneuploid cervical carcinoma HeLa cell line, and the primary diploid umbilical vein endothelial (HUVAC) cells with normal diploid XX karyotype. To assess the canonical trilayered suborganization of the nucleolus, we initially simultaneously codetected four distinct components of the FC, DFC, and GC subcompartments using super-resolved structured illumination microscopy (SR-SIM) imaging (Fig. 2a). To probe the organization of individual active rDNA transcription sites and the topology of rDNA genes in FCs across the whole nucleolus, we codetected the largest and catalytic subunit of RNA pol I complex RPA194 (Ford et al. 2023) and architectural chromatin factor UBF. UBF interacts with both the promoter and enhancer of rDNA genes. To further probe the structural interplay between the FC and DFC, we codetected these FC factors with NOLC1, which is highly accumulated in the DFC. NOLC1 interacts directly with RNA pol I (Chen et al. 1999) and provides a link between the site of pre-rRNA synthesis and cotranscriptional processing in the DFC via interactions with the rRNA modifying RNPs, the C/D box and H/ACA classes of snoRNPs (Yang et al. 2000). Moreover, to visualize the granular component, we detected nucleophosmin, a chaperone involved in the assembly steps of preribosomal subunits in GC (Mitrea et al. 2018) (Fig. 2a). Our SIM imaging revealed that prominent nucleoli in HeLa cells have reticulated patterns containing numerous small FC/DFC units scattered in evenly distributed arrangements throughout the whole nucleolar volume. Higher magnification demonstrated that FC/DFC units are organized as small ring-shaped structures. These structures partial overlay between UBF present in the core of FCs and active rDNA transcription sites marked with RPA194 protruding toward the periphery of the FC to DFC, which are detected by the presence of NOLC1 [Fig. 2a, two magnified regions (right, arrows); Fig. 2b].

To confirm our 3D SIM results, we used a novel Nikon NSPARC detection super-resolution microscopy to further resolve the 3D spatial suborganization of FC/DFC units within the entire nucleolar space. To ensure that the fiber-like transcription signals of RPA194 reflect all active rDNA genes, we codetected RPA194 with the Treacle (TCOF1) protein (Fig. 2c, left). TCOF1 has been recently proposed to act as a self-interacting factor solely required for the condensation of FC and scaffold for the RNA pol I transcription (independently of UBF) and its connection with enzymes responsible for ribosomal processing and modification (Lin and Yeh 2009; Jaberi-Lashkari et al. 2023). Furthermore, we codetected NOLC1 with another DFC marker, Dyskerin pseudouridine synthase 1 (a component of the H/ACA box snoRNPs), which is responsible for cotranscriptional modification of uridines to pseudouridines in the pre-rRNA (Garus and Autexier 2021) (Fig. 2c, right). NSPARC detection microscopy preventing possible *z*-drift revealed an almost complete 3D overlap between RPA194 and TCOF1 localizations and NOLC1 and Dyskerin signals projected within a whole nucleolar volume (Fig. 2c). Furthermore, we determined the average diameter of the individual active RNA pol I transcription sites detected by RPA194 as 190

± 40 nm. The surrounding DFCs, as measured by the NOLC1 signal, have a diameter of 335 ± 45 nm in our 3D images (Fig. 2d). These results indicate that small FC/DFC units are relatively uniform and evenly distributed, suborganized in a similar pattern and likely represent individual active ribosomal genes and pre-rRNA processing units.

To quantify the total number of transcription sites in proliferating diploid HUVAC cells, we employed similar 3D volume rendering, displaying SIM image volumes as 3D objects (Fig. 2e). On average, we detected ~115 distinct centrally-positioned transcription sites in total, per cell nucleus labeled by RPA194. These numbers agree with the number of individual active rDNA genes detected in human diploid lung fibroblasts IMR90 (Maiser et al. 2020). This observation suggests that one FC/DFC unit likely contains one or two active rDNA genes if we assume that up to 200 active rDNA genes are present at any given time in the human diploid genome (Fig. 2f). Consistent with these numbers, we detected, on average, ~175 small FC/DFC units per nucleus in malignant HeLa cells, which reflect a higher rDNA copy number due to aneuploidy of their genome (Yao et al. 2019) (Fig. 2e).

A structural suborganization of FC/DFC: a reticulated nucleolus versus nucleolus with an enlarged FCs

Notably, approximately 5–10% of HeLa cells display one or two prominent highly enlarged FCs in addition to typical small FC/DFC units in the nucleolus. Interestingly, some enlarged FCs are positioned inside the network of small FC/DFC units, but occasionally, they are located at an exclusive location outside the FC/DFC network in proximity. This suggests that some enlarged FCs might have different arrangements of rDNA repeat units or exclusive NOR topology. This is seen with RNA pol I transcription detected with RPA194 and codetected with DFC markers, NOLC1 and Dyskerin. The 28S rRNA detected by RNA FISH was predominantly in the GC and also in the DFC (Fig. 3a). These much larger FCs have been documented to have RNA pol I machinery predominantly localized by immunoelectron microscopy in FC interiors a few decades ago (Thiry and Goessens 1992). These observations led to longstanding debates about the precise intranucleolar localization of active rDNA genes with the claim of their exclusive location in the FC interior instead of at the FC boundary to DFC, as predicted in nucleoli with dozens of small FC/DFC units organized in the fiber-like network across the nucleolus (Fig. 2f) (Koberna et al. 2002). The enlarged FCs offer a unique opportunity for super-resolution microscopy to determine the principles of substructural spatial organization of active rDNA transcription sites and their physical link to the surrounding DFC (Fig. 3b, c). Additionally, the structural underpinnings of the FC as a platform for organizing active or silent rDNA loops from multiple chromosomes are still poorly understood. Our super-resolution four-color microscopy revealed that the enlarged FCs contained a larger number of transcriptionally active rDNA genes than found in the small FC/DFC units as detected by DNA FISH (Fig. 3d). Importantly, architectural FC protein TCOF1 is located in the inner core of the FCs, which might provide a scaffold for actively transcribing rDNA genes. Multiple engaged RNA pol I machineries, which resemble fiber-like patterns, protrude from the TCOP1-positive core FC region toward the boundary between the FC and DFC (Fig. 3b). Interestingly, NOLC1, is localized throughout the FC region, where it likely interacts with

the RNA pol I holoenzyme, but its location expands to the surrounding DFC, where it accumulates, as seen in the line scan profile (Fig. 3c). To assess the positions of active rDNA genes within larger FCs, we detected multiple rDNA genes by DNA FISH localized in FCs and boundary of FC/DFC. These results suggest that larger FCs likely have different rDNA topology with more internally located rDNA genes than small FC/DFC modules (Fig. 3d).

To assess the location of nascent 47S pre-rRNA synthesis in the enlarged FCs, we visualized the unstable 5′ETS leader sequence of 47S pre-rRNA upstream of the first cleavage site (A′ site) using RNA FISH. The 5′ETS leader RNA FISH signal was primarily detected in the DFC next to the RNA pol I location, which was at the periphery of the FC (Fig. 3e). This supports a view that nascent pre-rRNA transcript is rapidly redistributed to the DFC and likely stabilized by the recruitment of the SSU processome. Furthermore, to get an additional view of how the DFC is suborganized and where rRNA base modifications occur in the FC/DFC unit, we detected Dyskerin responsible for the modification of uridines to pseudouridines in the pre-rRNAs. Importantly, we observed that Dyskerin is almost exclusively detected within the DFC, suggesting that most pseudouridylation is restricted to the DFC (Fig. 3b, c). Even though NOLC1 and Dyskerin can be considered prototypical DFC markers, a combinatorial comparison of their topological intranuclear distributions indicates they are not homogeneous. NOLC1 is present not only in DFC but also in FC (Fig. 3c, line scan profile), where it links pre-rRNA synthesis with their processing. Importantly, these findings indicate that relative distributions of specific FC and DFC components are not exclusive and their substructural definitions must be open to a less exclusive interpretation and that needs further evaluation.

To visualize the granular component, we localized nucleophosmin, a chaperone involved in the assembly steps of preribosomal subunits in GC. Interestingly, nucleophosmin has a tubular appearance throughout the GC (Fig. 2a), where mature 18S (not shown) and 28S rRNA are detected (Figs. 3a, 4). To gain more information about the spatial distribution of pre-rRNA processing within the subcompartments of the nucleolus, we performed simultaneous multicolor RNA FISH hybridizing the 5′ETS leader sequence and the 28S rRNAs along with NOLC1 as a marker for the DFC (Fig. 4). The 5′ETS leader segment is primarily localized in DFC (Fig. 4, magnified regions, right) and processed in the inner parts of GC. The 28S rRNAs were detected in DFC regions as a part of nascent 47S primary transcript, consistent with wide-field microscopy [Lazdins et al. (1997)]. However, the rRNAs were predominantly located in tubular modules in the GC, frequently in very close proximity to each other. These results suggest that fully processed mature rRNAs, which act as backbones of small and large preribosomal subunits, can be frequently entangled even after their separation of the primary transcript, and that step-wise assembly of preribosomal particles, which begins with transcription initiation in the FC/DFC continues in the GC.

Nanostructural functional sub-organization of RNA pol I transcription sites by MINFLUX nanoscopy

To further investigate the nature of the functional suborganization of RNA pol I transcription sites in FCs, we used MINFLUX nanoscopy, which offers low nanometer-scale precision

localization of endogenous molecules. We recorded individual positions of RPA194 molecules within multiple individual small FCs initially detected by confocal microscopy in HeLa cells (Fig. 5a, b). X and Y coordinates were obtained by repeated localization for each blinking fluorophore molecule and grouped together into traces. The resulting data were filtered and processed to ensure each localized signal represented an individual protein. Analysis revealed that one small FC contains an average of 212.5 ± 30.1 individual RPA194 molecules (n = 17) (Fig. 5c). The number of the catalytic component RPA194 of RNA pol I detected in individual FCs by MINFLUX nanoscopy in HeLa cells agrees with our codetection data that small FC/DFC units are assembled on one or two transcriptionally active rDNA genes.

The framework of phase separation can be used to understand the local environment inside a dynamic organelle

A major outstanding question in the field is the extent to which structure and function of the nucleolus can be explained by a framework of liquid–liquid phase separation (LLPS) used to describe the nucleolus. On the one hand, each of the nucleolar subcompartments shows liquid-like properties, such as the ability to fuse and recover after photobleaching (Yao et al. 2019). Furthermore, many abundant nucleolar components have been shown to phase separate in vitro (Ferrolino et al. 2018; Mitrea et al. 2018; Lafontaine et al. 2021). On the other hand, ribosome maturation is inherently nonequilibrium, resulting in an outward flux of material and distinctly nonliquid-like characteristics, such as the rough outer edges of the GC.

To reconcile these views, valuable insights can be obtained from changes in the nucleolus observed upon the addition of RNA pol I inhibitors or other molecules that arrest pre-rRNA processing. These experiments reveal profound changes to nucleolar morphology, including coalescence of the FC/DFC units, smoothing of the outer edge of the GC, and even expulsion of the DFCs from the GC. We addressed this issue by visualization of the effect of BMH-21, which inhibits RNA pol I transcription by DNA intercalation (Wei et al. 2018), on the substructural organization of the nucleolus in HeLa cells using Nikon NSPARC 3D microscopy. Our results indicate that during short treatment with BMH-21, the nucleoli lose their irregularity, rough GC outer edges become roundish with a liquid-like appearance, and RNA pol I site coalesce and segregate from other subcompartments due to lack of ongoing pre-rRNA synthesis (Fig. 6). Thus, limiting the outward flux of pre-rRNA results in properties more typical of equilibrium liquids. A possible explanation for DFC coalescence, or lack thereof, is that partially transcribed rRNA molecules extend from the outer edge of the FC to the outer edge of the DFC, similar to the bristles of a brush. This “polymer brush” prevents the coalescence of FC/DFC units (Yamomoto et al. 2023). Reduction in metabolic activity causes this layer to thin, which allows FCs to merge until the FC core contains enough active transcriptional sites for the rRNA layer to arrest further coalescence.

The DFC layer is ~150–270 nm thick (Fig. 2d; Lafontaine et al. 2021), consistent with a single layer of pre-rRNA molecules still attached to the transcriptional machinery and undergoing cotranscriptional RNA folding, assembly and modification (Yamamoto et al.

2023). In contrast, the GC layer has a thickness on the order of 1 μm, which is much larger. Interestingly, pulse-chase experiments in the GC showed that the rRNA molecules undergo vectorial motion (Riback and Brangwynne 2020). This indicates that the diffusive contribution to motion is slow compared to the outward flux, possibly because the pre-rRNA molecules are highly entangled, they remain connected even when separated by vast distances (Riback and Brangwynne 2020). In contrast, FRAP experiments show that protein diffusion in the GC is relatively fast (Riback et al. 2023), suggesting that the protein environment around a given preribosomal particle can dynamically respond to the local folding/assembly state. This “local equilibrium” framework can be helpful in cases where certain molecular species are far from equilibrium while other species relax toward equilibrium rapidly (Schmit et al. 2020).

Structural biology additions and insights

Biochemistry, genetics, and cryoEM structural biology have made headway in piecing together a molecular stepwise model of ribosome biogenesis, beginning with yeast cells and continuing with recent advances using human cells (Vanden Broeck et al. 2022, 2023; Singh et al 2021). One limitation of such cryoEM studies is that intermediates are identified as either nucleolar, nuclear, or cytoplasmic and that it is currently not possible to identify which nucleolar regions these various intermediates reside in. Also, structural biology is limited because there is only a subset of intermediates known.

As the pre-rRNA transcript emerges from the RNA pol I, proteins and protein assemblies associate and dissociate to guide the folding of the emerging pre-rRNA (Fig. 7). A major challenge of RNA folding is the large stability of A-form helices, which can trap the misfolded RNA in the incorrect fold. To avoid rRNA misfolding, ribosome biogenesis uses several strategies to orchestrate a vectorial folding and assembly process. First, external, and internal transcribed spacers fold and assemble with numerous trans-acting factors to form a folding and assembly platform for early folding and assembly intermediates of the SSU and LSU rRNAs. Second, each successive assembly event creates new surfaces for binding and recruitment of the following protein factors or assemblies, thereby chaperoning the pre-rRNA to the subsequent folding and assembly step. Third, nucleotide-dependent ATP and GTP enzymes drive conformational changes through triphosphate hydrolysis. Fourth, site-specific endonucleases and nonspecific processive exonucleases drive this process irreversibly forward by removing external and internal transcribed spacer elements along with their associated trans-acting factors. There are also RNP and protein-based rRNA modification enzymes. Many of the snoRNP-driven modifications that occur during early steps in ribosome biogenesis are the result of chaperoning trans-acting factors that create a landing site for each snoRNP. Later, each snoRNP chemically modifies the rRNA and then dissociates to create new binding sites to recruit different trans-acting factors thereby driving the process in a highly regulated, cascading fashion forward.

RNA pol I structure

While there have been numerous studies of yeast pol I structures, structures of human RNA pol I have only been available since 2021 (Misiaszek et al 2021; Daiß et al. 2022). These

structures reveal that, similar to other polymerases, the fold and subunit architecture of this enzyme are remarkably similar throughout the eukaryotic kingdom despite low sequence identity. RNA pol II directly recruits mRNA processing machinery (5′ capping, pre-mRNA splicing, and 3′ end formation, including polyadenylation) that inevitably slows down rates of transcription. In contrast, RNA pol I is not similarly encumbered because this polymerase does not directly recruit pre-rRNA processing factors.

Structural intermediates in small subunit biogenesis

As the transcript first emerges from the exit tunnel on the RNA pol I, pre-rRNA folding and assembly begin with the association of both trans-acting factors and early binding RPs. The 5′ETS rRNA forms an RNP that creates a platform (the SSU processome) for folding and assembly of the small subunit RNP. The secondary structure of the four distinct structural domains of the 18S rRNA fold and assemble in sequential order as the pre-rRNA transcripts emerge from RNA pol I (Figs. 7, 8). These domains remain splayed apart in an open conformation, where much of the secondary structure is formed but limited mature tertiary interactions have yet to form (Fig. 8b, c). The open conformation is stabilized by interactions with the 5′ETS RNP and with the RNP chaperone, the U3 snoRNP. The latter snoRNA base pairs with the 5′ETS, the 5′ end of the 18S rRNA, and the 18S region between the central domain and the 3′ major domain. These U3-18S interactions sterically block the premature formation of a universal tertiary interaction, the central pseudoknot, until further folding and assembly have occurred (Fig. 8c).

After cleavage of a site within the 5′ETS (A0), exonuclease activity acts similar to a snowplow to simultaneously degrade this spacer element and dislodge all bound trans-acting factors (Fig. 8a). This action also exposes the mature 5′ end of the 18S rRNA and promotes its cleavage at A1 by an endonuclease. The resulting rearrangements create a surface that recruits the helicase DHX37, which then undocks the U3 snoRNP. Major domain rearrangement also takes place, notably of one of the four 18S domains (the 3′ minor domain) rotates by over 90 degrees along with rotation and folding of the other domains [Fig. 8b, compare pre-A1, post-A1, and state A structure 3′ minor domain (magenta)]. As the intermediate passes from the nucleolus to the nucleus the overall tertiary structure of the SSU takes shape and the central pseudoknot begins to form (Fig. 8b, c). The overall splaying and subsequent folding collapse of the SSU can be visualized by viewing the different stages of the folding of the central pseudoknot (Fig. 8c). The central pseudoknot starts with all the sequences in an open conformation in the pre-A1 structure, it is almost formed in the state A structure, and then, it finally folds in the mature structure. Subsequent rearrangements occur in the nucleus and cytoplasm, where quality control determines if the ribosome is fully functional and thus mature (Vanden Broeck et al. 2022, 2023; Singh et al 2021).

Structural intermediates in large subunit biogenesis

A fundamental difference between the folding of the rRNA of the SSU and that of the LSU is the number of folding domains. Whereas the SSU rRNA has four distinct structural domains the LSU has one giant domain composed of six interdigitating subdomains (Ban et al 2000) (Fig. 7). The combined cryoEM structural ribosome biogenesis intermediates

from yeast and human provide views of intermediates along the assembly pathway (Vanden Broeck et al. 2023). Many states are observed only in one of the two species. Both species have provided insight into the nucleolar structures, and humans have provided more nuclear structural intermediate structures (Fig. 8).

At the core of this massive LSU structure are six so-called root rRNA helices from each of these subdomains I through VI. Whereas half of the subdomains (1, 2, and 6) form some early secondary structures, the remaining subdomains gradually fold over the course of multiple intermediates (Vanden Broeck et al. 2023). Similar to SSU ribosome biogenesis, the irreversible assembly process involves stepwise trans-acting factor association and dissociation, structural rearrangements by ATP and GTP enzymes, and external and internal transcribed spacer element removal by endo- and exonucleases.

Anti-nucleolar therapies for the treatment of cancer

Inhibition of rDNA transcription by genotoxic agents

Despite the well-recognized roles of nucleolar function in cellular processes essential for tumorigenesis and cancer progression, drug development efforts targeting nucleolar components are limited. Such efforts have been appealing from the recognition decades ago that the number and shape of nucleoli are altered in cancer cells as well as the discovery that rRNA synthesis is upregulated in cancer and cancer metastasis. However, so far, anticancer drug development efforts targeting nucleolar function have been hampered by a narrow therapeutic window (Pianese and Teuscher 1896; Derenzini et al. 1998; Nguyen et al. 2015; Elhamamsy et al. 2022), as dose levels that are therapeutic and have antitumor efficacy are frequently too toxic to healthy cells and, thus, to patients. Treatment-limiting toxicities of genotoxic chemotherapy interfering with rDNA transcription agents go back to the discovery of actinomycin D in the 1960s (Zisi et al. 2022). This class of rDNA damaging agents activates the ribosomal biogenesis (RiBi) checkpoint of the nucleolus. Stalling of RNA pol I transcription, or impaired pre-rRNA processing, lowers levels of mature rRNA species in the nucleolus leading to a relative excess of RPs RPL5 and RPL11. This excess sequesters MDM2-E3 ubiquitin ligase, which under physiologic conditions targets p53 for proteasomal degradation (Bursac et al. 2021). Increased p53 levels upon RiBi checkpoint activation induce G2/M cell cycle arrest and apoptosis feeding into the genotoxic mechanism of action and activation of other DNA damage repair mechanisms of these agents. Agents such as mitomycin C exploit a more selective mechanism toward rDNA transcription-like crosslinking to GC-rich regions of rDNA genes or 5-fluorouracil (5-FU), which interferes with maturation of pre-rRNA. However, neither drug targets a unique nucleolar function that is present in cancer but absent from normal cells, which results in a narrow therapeutic window (Zisi et al. 2022).

Mutations in disordered proteins dysregulating BMCs and nucleolar function are enriched in cancer

A breakthrough in identifying a unique molecular mechanism associated with nucleolar dysfunction in cancer came from studying a rare congenital disease, brachyphalangy, polydactyly, and tibial aplasia syndrome (BPTAS). Mensah and coworkers have recently

shown that mutations in disordered proteins, and in particular, frameshift mutations that replace intrinsically disordered C-termini with arginine-rich basic tails destabilize LPPS and cause mispartitioning and subsequent dysfunction (Mensah et al. 2023). Importantly, these disease-causing mutations are not only enriched in families afflicted by BPTAS but also in other diseases including cancer (Bouchard et al. 2018; Mensah et al. 2023). Nucleoli of cells carrying mutations in intrinsically disordered regions (IDR) with frameshift-causing mutations in their C-terminus have abnormal phase transitions, altered fluidity, and dysregulated rRNA synthesis. Other nucleolar alterations associated with oncogenesis include abnormal rRNA 2′-O methylation post-transcriptional processessing, cancer mutations in the E3 ubiquitin ligase adaptor SPOP protein, which is also linked to abnormal LPPS, or mutated chaperone nucleophosmin (Marcel et al. 2020; White et al. 2019). Destabilized LPPS in the background of somatic or germline variants affecting IDR regions of nucleolar proteins might be a biomarker to select patients for antinucleolar therapies and might identify patients whose tumors are particularly responsive to oxaliplatin.

Oxaliplatin disrupts phase separation and inhibits rRNA synthesis

Despite many similarities between platinum analogues oxaliplatin (i.e., cisplatin and carboplatin including $\{Pt(NH_3)^{2+}\}$) that all cause intrastrand DNA crosslinks, different clinical activity profiles were observed within this class (Johnstone et al. 2016). Oxaliplatin is an FDA-approved first-line systemic chemotherapy for colorectal cancer and off label for other GI cancers, where it is often paired with 5-FU (Rottenberg et al. 2021). It has limited activity compared with other platinum agents in solid organ cancers of the lung or genitourinary system. Several recent studies have revealed a unique antinucleolar mechanism of oxaliplatin, which is disrupting LPPS (Bruno et al. 2017; Legin et al. 2020). Schmidt and coworkers showed that in comparison with actinomycin D and cisplatin, oxaliplatin alters nucleolar phase separation and changed fluid properties of the GC component from a complex to a more liquid phase via interference of fibrillarin phase separation-stabilizing function (Schmidt et al. 2022). Loss of LPPS reduced RNA pol I activity, which, within a feed-forward loop, accentuates further loss of separation between the DFC and the GC as pre-rRNA species are essential biomolecules for the maintenance of LLPS (Yao et al. 2019). Intriguingly, the antinucleolar mechanism of oxaliplatin explains the cooperativity of the drug with 5-FU, a chemotherapeutic known to also affect rRNA processing, which are administered in regimens such as FOLFOX or FOLFIRINOX. In this regard, the intimate association of ultrastructure and function of the nucleolus propelled by insights derived from novel applications of super-resolution light microscopy as presented in this paper has recently been shown to be associated with the drug phenotype of putative antinucleolar agents in a high-throughput drug screen. Different classes of agents were associated with different categories of nucleolar response subclassifying drug-induced nucleolar changes visualized by light microscopy beyond the “classical” stress reaction involving formation of nucleolar caps (Fig. 9) (Potapova et al. 2023). This work identified cyclin-dependent kinase (CDK) inhibitors and, in particular, CDK9 as a subclass of drugs inducing a unique state of nucleolar dissociation that might indicate a yet undiscovered role for targeting nucleolar function via this class of agents (Fig. 1a, b) (Sirri et al. 2002; Burger et al. 2013).

Drugs targeting rDNA transcription

So far, two small molecule inhibitors claimed to be inhibitors of RNA pol I transcription have reached clinical testing: CX-3543 and CX-5461 (Table 1).

CX-3543 and CX-5461

CX-3543 and CX-5461 were originally developed by Cylene Pharmaceutical (Ferreira et al. 2020). Neither compound targets cancer-specific alterations of rDNA transcription; rather, they were first used as stabilizers/modifiers of G-quadruplexes (Xu and Hurley 2022). G-quadruplexes are secondary structures of guanine-rich single DNA or RNA strands that are helical in shape and require the presence of repeat stretches of four or more consecutive guanines. Four guanine bases form a square, planar structure termed guanine tetrad, and several guanine tetrads stacked on top of each other form a G-quadruplex. G-quadruplexes have important biological function in genome organization and gene regulation, such as the protection of telomeres (Rhodes and Lipps 2015; Smirnov et al. 2023). CX-3543 was reported to have selectivity for G-quadruplex complexes at the rDNA promoter and did not affect telomere integrity (Drygin et al. 2009; Sanchez-Martin et al. 2021). CX-3543 was shown to cause loss of rDNA promotor binding of nucleolin, inhibit rDNA transcription, stabilize p53, and induce cell death. Due to poor bioavailability CX-3543 was withdrawn after phase I testing (Table 1).

CX-5461 was identified from a screen for inhibitors of rRNA transcription and initially thought to interfere with the polymerase I initiation complex before more recent studies identified it as a stabilizer of G4-quadruplexes (Xu et al. 2017; Xu and Hurley 2022). Stabilized G-quadruplexes via intercalation of CX-5461 induce replication fork stalling and unreplicated chromosomal areas, single-strand DNA breaks, and activate DNA damage repair (DDR) mechanisms, overall positioning the molecule as a topoisomerase 2 (TOP2) poison as opposed to a TOP2 inhibitor (Bruno et al. 2020; Pan et al. 2021). These insights have changed the trajectory of CX-5641's clinical development towards molecularly defined patient subgroup(s) with DNA repair deficiencies, such as BRCA1/2 or PALB2 (Xu and Hurley 2022). Results of the recently released phase I CCTG IND.231 trial showed several partial responses (Hilton et al. 2022). On the other hand, CX-5361 is an extraordinarily strong mutagen, and a phase IB expansion study is currently evaluating further safety and chronic tolerability of the molecule (Koh et al. 2024).

BMH-21 targeting RNA pol I

Another anti-pol I candidate is BMH-21. The liabilities of excessive DNA damage and a possible prohibitive mutagenesis potential do not apply to BMH-21. BMH-21 inhibits RNA pol I elongation after intercalation into GC-rich regions of rDNA genes and targets the released, the largest subunit of RNA polymerase I, RPA194, to proteasomal degradation (Peltonen et al. 2014a, b). BMH-21 does evoke activation of the RiBi checkpoint leading to p53 induction and programed cell death in the absence of induction of DNA damage (Peltonen et al. 2014b; Jacobs et al. 2022). BMH-21 is the first small molecule inhibitor directly targeting a component of the rDNA transcription machinery. BMH-21 was deemed unsuitable to be a clinical candidate due to off-target effects (Dorado et al. 2022).

Metarrestin

More recently, screens were developed to identify drugs that inhibited cancer specific changes in the nucleolus. Metarrestin was identified from a high-content screen targeting the perinucleolar compartment (PNC) (Frankowski et al. 2010, 2022), which is a marker of nuclear genome organization that is associated with the metastatic phenotype of cancer cells (Huang et al. 1997). PNCs are nearly universally found in metastatic cancer cells compared with cancer cells in primary tumors where they are less frequent. Importantly, PNCs are not observed in normal cells or stem cells (Kamath et al. 2005). Metarrestin showed impressive antimetastasis efficacy in preclinical models (Frankowski et al. 2018). While originally reported as a selective, PNC-targeting agent, metarrestin disassembles the PNC via its anti-RNA pol I activity (personal communication) as it inhibits transcription of RNA pol I-driven pyrimidine-rich noncoding transcript (PNCTR), an essential scaffold for the formation of the PNC, from the intergenic rDNA spacer (Yap et al. 2018). In comparison with CX-5461, metarrestin does not cause DNA damage and, in addition, fails to activate the RiBi checkpoint with no p53 induction observed across p53-wild type cell lines (Frankowski et al. 2018, 2022). The lack of p53 induction and cell death makes metarrestin a primarily cytostatic agent, which together with its favorable pharmacokinetic profile, might translate into an improved therapeutic window.

The development of effective therapeutics targeting rDNA transcription has been hampered by a lack of targets selective for the cancerous state. Future development of precision medicine strategies targeting rDNA transcription and nucleolar function will require the identification of cancer-specific nucleolar protein, rDNA, or pre-rRNA variants. As a first example, tying dysfunctional nucleolar partition due to mutations affecting IDR regions of nucleolar proteins to chemotypes, such as oxaliplatin already in clinical use, might be an immediately translatable strategy of a precision medicine approach against the nucleolus.

Conclusions

Ribosome biogenesis is fundamental to cell proliferation and, thus, to cancer cells as well, yet the molecular principles underlying this process remain poorly defined. Recent advances in microscopy have improved spatial resolution of substructural organization of the FC, DFC, and GC to provide detailed images of individual transcribing RNA pol I holoenzymes, quantitation of the number of FC/DFC units per nucleolus, and of nascent RNA pol I transcripts per FC. This more detailed view shows a heterogeneous distribution of factors throughout each subnucleolar layer, suggesting that these regions are not simple liquid–liquid phase separations but reflect a nonequilibrium vectorial path of the maturing ribosomal subunits. Our microscopic results together with recent super-resolution studies are augmented by recent Cryo EM structures of various human SSU and LSU intermediates (Vanden Broeck et al. 2023; Singh et al 2021; and reviewed in Vanden Broeck et al. 2022). Together with corresponding structures from yeast ribosomal intermediates, general principles are emerging that describe the irreversible folding, assembly, and rRNA processing steps that eventually produce mature ribosomes in the cytoplasm. Lastly, previous generation drugs that target ribosome biogenesis were of limited use due to their toxicity; however, newer drugs that target cancer specific changes in the nucleolus have

rekindled the interest in antinucleolar treatment strategies that target cancer cells and spare normal cells as effective cancer therapies.

Materials and methods

Hybridization probes

The DNA hybridization probe was generated using a 5.6 kb EcoRI-EcoRI human rDNA fragment-containing promoter, 5′ETS, and 18S rDNA and labeled by nick translation with 552-dUTP from Biotium.

DNA FISH

HeLa cells grown on 1.5H precision 12-mm circle coverslips were washed with PBS and fixed with 4% PFA in PBS for 10 min at room temperature. After rinsing in PBS, cells were permeabilized with 0.2% Triton X-100, 0.5% saponin in PBS for 20 min on ice, and washed with PBS. Subsequently, the cells were incubated in 0.1 N HCl for 15 min, then washed twice in 2× SSC for 10 min, before equilibration in 50% formamide/2× SSC for 30 min. For one 12 mm round coverslip, ~150 ng of DNA FISH probe was precipitated with 3 μg of Cot-1 DNA (Roche) and 1 μg of yeast tRNA in ice-cold absolute ethanol by sodium acetate, spun down, dried, and resuspended in 7 μl of hybridization solution (10% dextran sulfate/50% formamide (pH 7.0)/2 × SSC/1% Tween20). The cocktail was denatured at 85 °C for 5 min, put briefly on ice, incubated with cells at 85 °C for 5 min, sealed with rubber cement, and hybridized in a humidified chamber overnight at 37 °C. After hybridization, cells were washed three times in 50% formamide/2× SSC for 5 min at 45 °C, washed three times in 1× SSC for 5 min at 60 °C and in PBS for 5 min. Then, cells were incubated with specific antibodies for 1 h and washed three times in PBS. Cells were washed three times in PBS for 5 min, and mounted using ProLong Gold antifade mounting reagent without DAPI (ThermoFisher). Cells were observed on a Zeiss Elyra SIM microscope using a 63 × 1.40 NA objective using *z*-sectioning (*z*-0.92 nm), five rotations, processed and aligned using the TetraSpeck fluorescent beads (Invitrogen) with Zeiss Zen software.

Immunofluorescence and super-resolution microscopy

HeLa cells and primary diploid umbilical vein endothelial (HUVAC) cells with normal diploid XX karyotype were grown on 1.5H precision 12-mm circle coverslips. Cells were fixed with 4% PFA in PBS for 10 min at room temperature. After rinsing in PBS, cells were permeabilized with 0.2% Triton X-100 in PBS for 5 min on ice and were washed with PBS. Cells were blocked with 3% BSA and labeled with labeled antibodies for one hour at room temperature. Then, they were washed in PBS and mounted using ProLong Gold antifade mounting reagent without DAPI (ThermoFisher) or Vectashield without DAPI. The slides were visualized using super-resolution SIM Zeiss Elyra using 63× objective 1.4 NA with ~110 nm resolution (*XY*) and confocal Nikon AXR microscope with an NSPARC detector with single-photon level sensitivity and improved resolution to ~100 nm (*XY*) and 300 nm (*Z*) using 100× objective 1.45 NA. The SIM images were processed using Zeiss Zen software and corrected by channel alignment using the TetraSpeck fluorescent beads (Invitrogen).

3D rendering and measurements

3D renderings were generated using the surface rendering feature of Huygens Essential (Scientific Volume Imaging, BV, Netherlands). Huygens object analysis feature was also used to count the number of transcription sites within the FCs. We measured the diameter of RNA pol I transcription sites detected by RPA194 and the diameter of DFC detected by Dyskerin in our 3D images of HUVAC cells visualized on Nikon AXR microscope using full width at half maximum intensity using Nikon software.

RNA FISH

All single molecule RNA FISH LNA oligo probes were labeled with green and red fluorophores on the 3′ ends. Cells were grown on 1.5H precision 12 mm circle coverslips and fixed with 4% PFA for 10 min, followed by permeabilization with 0.5% Triton X-100 on ice for 5 min. Cells were incubated in 10% formamide/2× SSC for 10 min at room temperature, followed by hybridization overnight at 37 °C. After hybridization, the cells were blocked with 3% BSA for 20 min and incubated with antibodies, as described above. Coverslips were mounted in ProLong Gold antifade mounting medium (ThermoFisher).

MINFLUX nanoscopy

HeLa cells were grown on 1.5H precision 18-mm circle coverslips. After fixation with 4% PFA, the cells were labeled with the mouse monoclonal anti-RPA194 antibody and then with the secondary anti-mouse IgG antibody coupled with Alexa 647. Coverslips were mounted into the buffer with 18.8 mM beta-mercaptoethylamine and oxygen scavengers [50 mM Tris–HCl (pH 8.0), 10 mM NaCl, 10% (w/v) glucose, 64 µg/ml catalase (Sigma-Aldrich), and 0.4 mg/ml glucose oxidase (Sigma-Aldrich)] to regulate photo blinking of Alexa 647. To correct for XYZ drift, 150 nm gold bead fiducials were applied to the coverslip prior to mounting (BBI solution, SKU EM. GC150). The samples were sealed with silicone glue and imaged. 2D MINFLUX (Abberior, Germany) measurements were performed with a 647 laser at 19 mW in the first iteration and a pinhole size of 0.83 AU. Data from MINFLUX consist of coordinates obtained by repeated localization for each single molecule of fluorophore that are grouped together into traces. Any trace that contained less than five localizations was discarded to remove localizations due to noise. A single position for each remaining trace was obtained by taking the average X and Y coordinates of the localizations within the trace.

The MINFLUX technique provides multiple localizations for a single fluorophore, called a trace. Each RPA194 molecule could be decorated with multiple fluorophores, thus detected by one to three traces, and each single fluorophore may produce multiple traces due to “blinking” or repeated transitioning between the dark and fluorescent states. To avoid the over-counting that would result from these two situations, the averaged trace positions were combined by applying a density-based clustering algorithm (dbscan), with a distance parameter of 3.5 nm, corresponding to the localization precision of MINFLUX. Such a cluster contains localizations of one to three molecules in close proximity. Trace coordinates within each cluster were then averaged to obtain the position of each molecule. This allows the approximate localization of a single RPA194 molecule detected by several fluorophores/blinks. After that, we searched for the clusters of these RPA194 molecules. To group

RPA194 molecules within each FC, the localized molecules were further clustered with dbscan with a distance parameter set to 60 nm and a minimum number of localizations set to 15.

Acknowledgements

We are grateful to Rosalind Franklin University of Medicine and Science for the support of our studies. This research was funded by NIH 1R01GM141235 and the Intramural Research Program of the National Institutes of Health (NIH), National Cancer Institute (NCI), Center for Cancer Research (CCR) (ZIA BC 011267). We thank Dr. Michael Davis for providing the bead measurements for Nikon AXR NSPARC microscopy. The opinions expressed in this article are the authors own and do not reflect the view of the National Institutes of Health, the Department of Health and Human Services, or the US Government, nor does mention of trade names, commercial products, or organization imply endorsement by the US Government. We sincerely apologize to our colleagues whose work could not be cited due to space limitations.

Data availability

No datasets were generated or analysed during the current study.

References

Azouzi C, Jaafar M, Dez C, Abou Merhi R, Lesne A, Henras AK, Gadal O (2021) Coupling between production of ribosomal RNA and maturation: just at the beginning. Front Mol Biosci 8:778778. 10.3389/fmolb.2021.778778 [PubMed: 34765647]

Ban N, Nissen P, Hansen J, Moore PB, Steitz TA (2000) The complete atomic structure of the large ribosomal subunit at 2.4 a resolution. Science. 289(5481):905–20. 10.1126/science.289.5481.905 [PubMed: 10937989]

Bizhanova A, Kaufman PD (2021) Close to the edge: Heterochromatin at the nucleolar and nuclear peripheries. Biochim Biophys Acta Gene Regul Mech. 1864(1):194666. 10.1016/j.bbagrm.2020.194666 [PubMed: 33307247]

Boulon S, Westman BJ, Hutten S, Boisvert FM, Lamond AI (2010) The nucleolus under stress. Mol Cell 40(2):216–227. 10.1016/j.molcel.2010.09.024 [PubMed: 20965417]

Bruno PM, Liu Y, Park GY, Murai J, Koch CE, Eisen TJ, Pritchard JR, Pommier Y, Lippard SJ, Hemann MT (2017) A subset of platinum-containing chemotherapeutic agents kills cells by inducing ribosome biogenesis stress. Nat Med. 23(4):461—471. 10.1038/nm.4291 [PubMed: 28263311]

Burger K, Mühl B, Rohrmoser M, Coordes B, Heidemann M, Kellner M, Gruber-Eber A, Heissmeyer V, Strässer K, Eick D (2013) Cyclin-dependent kinase 9 links RNA polymerase II transcription to processing of ribosomal RNA. J Biol Chem. 288(29):21173–21183. 10.1074/jbc.M113.483719 [PubMed: 23744076]

Bursać S, Prodan Y, Pullen N, Bartek J, Volarević S (2021) Dysregulated ribosome biogenesis reveals therapeutic liabilities in cancer. Trends Cancer 7(1):57–76. 10.1016/j.trecan.2020.08.003 [PubMed: 32948502]

Chen HK, Pai CY, Huang JY, Yeh NH (1999) Human Nopp140, which interacts with RNA polymerase I: implications for rRNA gene transcription and nucleolar structural organization. Mol Cell Biol 19(12):8536–8546. 10.1128/MCB.19.12.8536 [PubMed: 10567578]

Correll CC, Bartek J, Dundr M (2019) The nucleolus: a multiphase condensate balancing ribosome synthesis and translational capacity in health aging and ribosomopathies. Cells 8(8):869. 10.3390/cells8080869 [PubMed: 31405125]

Daiß JL, Pilsl M, Straub K, Bleckmann A, Höcherl M, Heiss FB, Abascal-Palacios G, Ramsay EP, Tlučková K, Mars JC, Fürtges T, Bruckmann A, Rudack T, Bernecky C, Lamour V, Panov K, Vannini A, Moss T, Engel C (2022) The human RNA polymerase I structure reveals an HMG-like docking domain specific to metazoans. Life Sci Alliance 5(11):e202201568. 10.26508/lsa.202201568 [PubMed: 36271492]

Denissov S, Lessard F, Mayer C, Stefanovsky V, van Driel M, Grummt I, Moss T, Stunnenberg HG (2011) A model for the topology of active ribosomal RNA genes. EMBO Rep 12(3):231–237. 10.1038/embor.2011.8 [PubMed: 21331097]

Derenzini M, Trerè D, Pession A, Montanaro L, Sirri V, Ochs RL (1998) Nucleolar function and size in cancer cells. Am J Pathol. 152(5):1291–7 [PubMed: 9588897]

Dorado TE, de León P, Begum A, Liu H, Chen D, Rajeshkumar NV, Rey-Rodriguez R, Hoareau-Aveilla C, Alcouffe C, Laiho M, Barrow JC (2022) Discovery and evaluation of novel angular fused pyridoquinazolinonecarboxamides as RNA polymerase I inhibitors. ACS Med Chem Lett 13(4):608–614. 10.1021/acsmedchemlett.1c00660 [PubMed: 35450366]

Drygin D, Siddiqui-Jain A, O'Brien S, Schwaebe M, Lin A, Bliesath J, Ho CB, Proffitt C, Trent K, Whitten JP, Lim JK, Von Hoff D, Anderes K, Rice WG (2009) Anticancer activity of CX-3543: a direct inhibitor of rRNA biogenesis. Cancer Res 69(19):7653–7661. 10.1158/0008-5472.CAN-09-1304 [PubMed: 19738048]

Dundr M, Olson MO (1998) Partially processed pre-rRNA is preserved in association with processing components in nucleolus-derived foci during mitosis. Mol Biol Cell 9(9):2407–2422. 10.1091/mbc.9.9.2407 [PubMed: 9725903]

Dundr M, Hoffmann-Rohrer U, Hu Q, Grummt I, Rothblum LI, Phair RD, Misteli T (2002) A kinetic framework for a mammalian RNA polymerase in vivo. Science 298(5598):1623–1626. 10.1126/science.1076164 [PubMed: 12446911]

Elhamamsy AR, Metge BJ, Alsheikh HA, Shevde LA, Samant RS (2022) Ribosome biogenesis: a central player in cancer metastasis and therapeutic resistance. Cancer Res 82(13):2344–2353. 10.1158/0008-5472.CAN-21-4087 [PubMed: 35303060]

Ferreira R, Schneekloth JS Jr, Panov KI, Hannan KM, Hannan RD (2020) Targeting the RNA polymerase I transcription for cancer therapy comes of age. Cells 9(2):266. 10.3390/cells9020266 [PubMed: 31973211]

Ferrolino MC, Mitrea DM, Michael JR, Kriwacki RW (2018) Compositional adaptability in NPM1-SURF6 scaffolding networks enabled by dynamic switching of phase separation mechanisms. Nat Commun 9(1):5064. 10.1038/s41467-018-07530-1 [PubMed: 30498217]

Ford BL, Wei T, Liu H, Scull CE, Najmi SM, Pitts S, Fan W, Schneider DA, Laiho M (2023) Expression of RNA polymerase I catalytic core is influenced by RPA12. PLoS ONE 18(5):e0285660. 10.1371/journal.pone.0285660 [PubMed: 37167337]

Frankowski KJ, Wang C, Patnaik S, Schoenen FJ, Southall N, Li D, Teper Y, Sun W, Kandela I, Hu D, Dextras C, Knotts Z, Bian Y, Norton J, Titus S, Lewandowska MA, Wen Y, Farley KI, Griner LM, Sultan J, Meng Z, Zhou M, Vilimas T, Powers AS, Kozlov S, Nagashima K, Quadri HS, Fang M, Long C, Khanolkar O, Chen W, Kang J, Huang H, Chow E, Goldberg E, Feldman C, Xi R, Kim HR, Sahagian G, Baserga SJ, Mazar A, Ferrer M, Zheng W, Shilatifard A, Aubé J, Rudloff U, Marugan JJ, Huang S (2018) Metarrestin, a perinucleolar compartment inhibitor, effectively suppresses metastasis. Sci Transl Med. 10(441):eaap8307. 10.1126/scitranslmed.aap8307 [PubMed: 29769289]

Frankowski KJ, Patnaik S, Wang C, Southall N, Dutta D, De S, Li D, Dextras C, Lin YH, Bryant-Connah M, Davis D, Wang F, Wachsmuth LM, Shah P, Williams J, Kabir M, Zhu E, Baljinnyam B, Wang A, Xu X, Norton J, Ferrer M, Titus S, Simeonov A, Zheng W, Mathews Griner LA, Jadhav A, Aubé J, Henderson MJ, Rudloff U, Schoenen FJ, Huang S, Marugan JJ (2022) Discovery and optimization of pyrrolopyrimidine derivatives as selective disruptors of the perinucleolar compartment, a marker of tumor progression toward metastasis. J Med Chem. 65(12):8303—8331. 10.1021/acs.jmedchem.2c00204 [PubMed: 35696646]

Frankowski K, Patnaik S, Schoenen F, Huang S, Norton J, Wang C, Titus S, Ferrer M, Zheng W, Southall N, Day VW, Aubé J, Marugan JJ. (2010) Discovery and Development of Small Molecules That Reduce PNC Prevalence. In: Probe Reports from the NIH Molecular Libraries Program [Internet]. Bethesda (MD): National Center for Biotechnology Information (US); 2010.

Fu Y, Liu Y, Wen T, Fang J, Chen Y, Zhou Z, Gu X, Wu H, Sheng J, Xu Z, Zou W, Chen B (2023) Real-time imaging of RNA polymerase I activity in living human cells. J Cell Biol. 222(1):e202202110. 10.1083/jcb.202202110 [PubMed: 36282216]

Gagnon-Kugler T, Langlois F, Stefanovsky V, Lessard F, Moss T (2009) Loss of human ribosomal gene CpG methylation enhances cryptic RNA polymerase II transcription and disrupts ribosomal RNA processing. Mol Cell 35(4):414–425. 10.1016/j.molcel.2009.07.008 [PubMed: 19716787]

Garus A, Autexier C (2021) Dyskerin: an essential pseudouridine synthase with multifaceted roles in ribosome biogenesis, splicing, and telomere maintenance. RNA. 12:1441–1458. 10.1261/rna.078953.121

Hilton J, Gelmon K, Bedard PL, Tu D, Xu H, Tinker AV, Goodwin R, Laurie SA, Jonker D, Hansen AR, Veitch ZW, Renouf DJ, Hagerman L, Lui H, Chen B, Kellar D, Li I, Lee SE, Kono T, Cheng BYC, Yap D, Lai D, Beatty S, Soong J, Pritchard KI, Soria-Bretones I, Chen E, Feilotter H, Rushton M, Seymour L, Aparicio S, Cescon DW (2022) Results of the phase I CCTG IND.231 trial of CX-5461 in patients with advanced solid tumors enriched for DNA-repair deficiencies. Nat Commun. 13(1):3607. 10.1038/s41467-022-31199-2 [PubMed: 35750695]

Hirose T, Ninomiya K, Nakagawa S, Yamazaki T (2023) A guide to membraneless organelles and their various roles in gene regulation. Nat Rev Mol Cell Biol 24(4):288–304. 10.1038/s41580-022-00558-8 [PubMed: 36424481]

Huang S, Deerinck TJ, Ellisman MH, Spector DL (1997) The dynamic organization of the perinucleolar compartment in the cell nucleus. J Cell Biol 137(5):965–974. 10.1083/jcb.137.5.965 [PubMed: 9166399]

Jacobs RQ, Huffines AK, Laiho M, Schneider DA (2022) The small-molecule BMH-21 directly inhibits transcription elongation and DNA occupancy of RNA polymerase I in vivo and in vitro. J Biol Chem. 298(1):101450. 10.1016/j.jbc.2021.101450 [PubMed: 34838819]

Johnstone TC, Suntharalingam K, Lippard SJ (2016) The next generation of platinum drugs: targeted Pt(II) agents, nanoparticle delivery, and Pt(IV) prodrugs. Chem Rev. 116(5):3436–86. 10.1021/acs.chemrev.5b00597 [PubMed: 26865551]

Kamath RV, Thor AD, Wang C, Edgerton SM, Slusarczyk A, Leary DJ, Wang J, Wiley EL, Jovanovic B, Wu Q, Nayar R, Kovarik P, Shi F, Huang S (2005) Perinucleolar compartment prevalence has an independent prognostic value for breast cancer. Cancer Res 65(1):246–253 [PubMed: 15665301]

Koberna K, Malínský J, Pliss A, Masata M, Vecerova J, Fialová M, Bednár J, Raska I (2002) Ribosomal genes in focus: new transcripts label the dense fibrillar components and form clusters indicative of “Christmas trees” in situ. J Cell Biol. 157(5):743–8. 10.1083/jcb.200202007 [PubMed: 12034768]

Koh GCC, Boushaki S, Zhao SJ, Pregnall AM, Sadiyah F, Badja C, Memari Y, Georgakopoulos-Soares I, Nik-Zainal S (2024) The chemotherapeutic drug CX-5461 is a potent mutagen in cultured human cells. Nat Genet. 56(1):23–26. 10.1038/s41588-023-01602-9 [PubMed: 38036782]

Kresoja-Rakic J, Santoro R (2019) Nucleolus and rRNA gene chromatin in early embryo development. Trends Genet. 35(11):868–879. 10.1016/j.tig.2019.06.005 [PubMed: 31327501]

Kufel J, Grzechnik P (2019) Small nucleolar RNAs tell a different tale. Trends Genet. 35(2):104–117. 10.1016/j.tig.2018.11.005 [PubMed: 30563726]

Lafontaine DLJ, Riback JA, Bascetin R, Brangwynne CP (2021) The nucleolus as a multiphase liquid condensate. Nat Rev Mol Cell Biol 22(3):165–182. 10.1038/s41580-020-0272-6 [PubMed: 32873929]

le Nguyen XT, Raval A, Garcia JS, Mitchell BS (2015) Regulation of ribosomal gene expression in cancer. J Cell Physiol 230(6):1181–1188. 10.1002/jcp.24854 [PubMed: 25336383]

Legin AA, Schintlmeister A, Sommerfeld NS, Eckhard M, Theiner S, Reipert S, Strohhofer D, Jakupec MA, Galanski MS, Wagner M, Keppler BK (2020) Nano-scale imaging of dual stable isotope labeled oxaliplatin in human colon cancer cells reveals the nucleolus as a putative node for therapeutic effect. Nanoscale Adv 3(1):249–262. 10.1039/d0na00685h [PubMed: 36131874]

Lin CI, Yeh NH (2009) Treacle recruits RNA polymerase I complex to the nucleolus that is independent of UBF. Biochem Biophys Res Commun 386(2):396–401. 10.1016/j.bbrc.2009.06.050 [PubMed: 19527688]

Lindström MS, Jurada D, Bursac S, Orsolic I, Bartek J, Volarevic S (2018) Nucleolus as an emerging hub in maintenance of genome stability and cancer pathogenesis. Oncogene. 37(18):2351–2366. 10.1038/s41388-017-0121-z [PubMed: 29429989]

Maiser A, Dillinger S, Längst G, Schermelleh L, Leonhardt H, Németh A (2020) Super-resolution in situ analysis of active ribosomal DNA chromatin organization in the nucleolus. Sci Rep 10(1):7462. 10.1038/s41598-020-64589-x [PubMed: 32366902]

Marcel V, Kielbassa J, Marchand V, Natchiar KS, Paraqindes H, Nguyen Van Long F, Ayadi L, Bourguignon-Igel V, Lo Monaco P, Monchiet D, Scott V, Tonon L, Bray SE, Diot A, Jordan LB, Thompson AM, Bourdon JC, Dubois T, André F, Catez F, Puisieux A, Motorin Y, Klaholz BP, Viari A, Diaz JJ (2020) Ribosomal RNA 2'O-methylation as a novel layer of inter-tumour heterogeneity in breast cancer. NAR Cancer. 2(4):036. 10.1093/narcan/zcaa036.(Erratum in: NAR Cancer. 2021 Feb 22;3(1):zcab006) [PubMed: 34319295]

Mensah MA, Niskanen H, Magalhaes AP, Basu S, Kircher M, Sczakiel HL, Reiter AMV, Elsner J, Meinecke P, Biskup S, Chung BHY, Dombrowsky G, Eckmann-Scholz C, Hitz MP, Hoischen A, Holterhus PM, Hülsemann W, Kahrizi K, Kalscheuer VM, Kan A, Krumbiegel M, Kurth I, Leubner J, Longardt AC, Moritz JD, Najmabadi H, Skipalova K, Snijders Blok L, Tzschach A, Wiedersberg E, Zenker M, Garcia-Cabau C, Buschow R, Salvatella X, Kraushar ML, Mundlos S, Caliebe A, Spielmann M, Horn D, Hnisz D (2023) Aberrant phase separation and nucleolar dysfunction in rare genetic diseases. Nature. 2614(7948):564–571. 10.1038/s41586-022-05682-1

Misiaszek AD, Girbig M, Grötsch H, Baudin F, Murciano B, Lafita A, Müller CW (2021) Cryo-EM structures of human RNA polymerase I. Nat Struct Mol Biol. 28(12):997–1008. 10.1038/s41594-021-00693-4 [PubMed: 34887565]

Mitrea DM, Cika JA, Stanley CB, Nourse A, Onuchic PL, Banerjee PR, Phillips AH, Park CG, Deniz AA, Kriwacki RW (2018) Self-interaction of NPM1 modulates multiple mechanisms of liquid-liquid phase separation. Nat Commun 9(1):842. 10.1038/s41467-018-03255-3 [PubMed: 29483575]

Miyake T, McDermott JC (2023) Re-organization of nucleolar architecture in myogenic differentiation. J Cell Sci. 136(4):jcs260496. 10.1242/jcs.260496 [PubMed: 36727534]

Nelson JO, Watase GJ, Warsinger-Pepe N, Yamashita YM (2019) Mechanisms of rDNA copy number maintenance. Trends Genet. 35(10):734–742. 10.1016/j.tig.2019.07.006 [PubMed: 31395390]

Nurk S, Koren S, Rhie A, Rautiainen M, Bzikadze AV, Mikheenko A, Vollger MR, Altemose N, Uralsky L, Gershman A, Aganezov S, Hoyt SJ, Diekhans M, Logsdon GA, Alonge M, Antonarakis SE, Borchers M, Bouffard GG, Brooks SY, Caldas GV, Chen NC, Cheng H, Chin CS, Chow W, de Lima LG, Dishuck PC, Durbin R, Dvorkina T, Fiddes IT, Formenti G, Fulton RS, Fungtammasan A, Garrison E, Grady PGS, Graves-Lindsay TA, Hall IM, Hansen NF, Hartley GA, Haukness M, Howe K, Hunkapiller MW, Jain C, Jain M, Jarvis ED, Kerpedjiev P, Kirsche M, Kolmogorov M, Korlach J, Kremitzki M, Li H, Maduro VV, Marschall T, McCartney AM, McDaniel J, Miller DE, Mullikin JC, Myers EW, Olson ND, Paten B, Peluso P, Pevzner PA, Porubsky D, Potapova T, Rogaev EI, Rosenfeld JA, Salzberg SL, Schneider VA, Sedlazeck FJ, Shafin K, Shew CJ, Shumate A, Sims Y, Smit AFA, Soto DC, Sović I, Storer JM, Streets A, Sullivan BA, Thibaud-Nissen F, Torrance J, Wagner J, Walenz BP, Wenger A, Wood JMD, Xiao C, Yan SM, Young AC, Zarate S, Surti U, McCoy RC, Dennis MY, Alexandrov IA, Gerton JL, O'Neill RJ, Timp W, Zook JM, Schatz MC, Eichler EE, Miga KH, Phillippy AM (2022) The complete sequence of a human genome. Science. 376(6588):44–53. 10.1126/science.abj6987 [PubMed: 35357919]

Olson MO, Dundr M (2005) The moving parts of the nucleolus. Histochem Cell Biol 123(3):203–216. 10.1007/s00418-005-0754-9 [PubMed: 15742198]

Pan M, Wright WC, Chapple RH, Zubair A, Sandhu M, Batchelder JE, Huddle BC, Low J, Blankenship KB, Wang Y, Gordon B, Archer P, Brady SW, Natarajan S, Posgai MJ, Schuetz J, Miller D, Kalathur R, Chen S, Connelly JP, Babu MM, Dyer MA, Pruett-Miller SM, Freeman BB 3rd, Chen T, Godley LA, Blanchard SC, Stewart E, Easton J, Geeleher P (2021) The chemotherapeutic CX-5461 primarily targets TOP2B and exhibits selective activity in high-risk neuroblastoma. Nat Commun 12(1):6468. 10.1038/s41467-021-26640-x [PubMed: 34753908]

Parks MM, Kurylo CM, Dass RA, Bojmar L, Lyden D, Vincent CT, Blanchard SC (2018) Variant ribosomal RNA alleles are conserved and exhibit tissue-specific expression. Sci Adv. 4(2):eaao0665. 10.1126/sciadv.aao0665 [PubMed: 29503865]

Pederson T (2011) The nucleolus. Cold Spring Harb Perspect Biol 3(3):a000638. 10.1101/cshperspect.a000638 [PubMed: 21106648]

Peltonen K, Colis L, Liu H, Jäämaa S, Zhang Z, Af Hällström T, Moore HM, Sirajuddin P, Laiho M (2014a) Small molecule BMH-compounds that inhibit RNA polymerase I and cause nucleolar stress. Mol Cancer Ther. 13(11):2537–46. 10.1158/1535-7163.MCT-14-0256 [PubMed: 25277384]

Peltonen K, Colis L, Liu H, Trivedi R, Moubarek MS, Moore HM, Bai B, Rudek MA, Bieberich CJ, Laiho M (2014b) A targeting modality for destruction of RNA polymerase I that possesses anticancer activity. Cancer Cell 25(1):77–90. 10.1016/j.ccr.2013.12.009 [PubMed: 24434211]

Penzo M, Montanaro L, Treré D, Derenzini M (2019) The ribosome biogenesis-cancer connection. Cells 8(1):55. 10.3390/cells8010055 [PubMed: 30650663]

Pianese R, Teuscher R (1896) Beitrag Zur Histologie Und Aetiologie Des Carcinoms: Histologische Und Experimentelle Untersuchungen. Beitr Pathol Anat 142:1–193

Potapova TA, Unruh JR, Conkright-Fincham J, Banks CAS, Florens L, Schneider DA, Gerton JL (2023) Distinct states of nucleolar stress induced by anticancer drugs. Elife. 12:RP88799. 10.7554/eLife.88799 [PubMed: 38099650]

Rhodes D, Lipps HJ (2015) G-quadruplexes and their regulatory roles in biology. Nucleic Acids Res. 43(18):8627–37. 10.1093/nar/gkv862 [PubMed: 26350216]

Riback JA, Brangwynne CP (2020) Can phase separation buffer cellular noise? Science 367(6476):364–365. 10.1126/science.aba0446 [PubMed: 31974233]

Riback JA, Eeftens JM, Lee DSW, Quinodoz SA, Donlic A, Orlovsky N, Wiesner L, Beckers L, Becker LA, Strom AR, Rana U, Tolbert M, Purse BW, Kleiner R, Kriwacki R, Brangwynne CP (2023) Viscoelasticity and advective flow of RNA underlies nucleolar form and function. Mol Cell 83(17):3095–3107.e9. 10.1016/j.molcel.2023.08.006 [PubMed: 37683610]

Rottenberg S, Disler C, Perego P (2021) The rediscovery of platinum-based cancer therapy. Nat Rev Cancer 21(1):37–50. 10.1038/s41568-020-00308-y [PubMed: 33128031]

Sanchez-Martin V, Soriano M, Garcia-Salcedo JA (2021) Quadruplex ligands in cancer therapy. Cancers (Basel) 13(13):3156. 10.3390/cancers13133156 [PubMed: 34202648]

Sawyer IA, Sturgill D, Dundr M (2019) Membraneless nuclear organelles and the search for phases within phases. Wiley Interdiscip Rev RNA 10(2):e1514. 10.1002/wrna.1514 [PubMed: 30362243]

Schmidt HB, Jaafar ZA, Wulff BE, Rodencal JJ, Hong K, Aziz-Zanjani MO, Jackson PK, Leonetti MD, Dixon SJ, Rohatgi R, Brandman O (2022) Oxaliplatin disrupts nucleolar function through biophysical disintegration. Cell Rep 41(6):111629. 10.1016/j.celrep.2022.111629 [PubMed: 36351392]

Schmit JD, Bouchard JJ, Martin EW, Mittag T (2020) Protein network structure enables switching between liquid and gel states. J Am Chem Soc. 142(2):874–883. 10.1021/jacs.9b10066 [PubMed: 31845799]

Singh S, Vanden Broeck A, Miller L, Chaker-Margot M, Klinge S (2021) Nucleolar maturation of the human small subunit processome. Science. 373(6560):eabj5338. 10.1126/science.abj5338 [PubMed: 34516797]

Sirri V, Jourdan N, Hernandez-Verdun D, Roussel P (2016) Sharing of mitotic pre-ribosomal particles between daughter cells. J Cell Sci 129(8):1592–1604. 10.1242/jcs.180521 [PubMed: 26929073]

Sloan KE, Warda AS, Sharma S, Entian KD, Lafontaine DLJ, Bohnsack MT (2017) Tuning the ribosome: the influence of rRNA modification on eukaryotic ribosome biogenesis and function. RNA Biol. 14(9):1138–1152. 10.1080/15476286.2016.1259781 [PubMed: 27911188]

Smirnov E, Molínová P, Chmúrčiaková N, Vacík T, Cmarko D (2023) Non-canonical DNA structures in the human ribosomal DNA. Histochem Cell Biol 160(6):499–515. 10.1007/s00418-023-02233-1 [PubMed: 37750997]

Srivastava R, Srivastava R, Ahn SH (2016) The epigenetic pathways to ribosomal DNA silencing. Microbiol Mol Biol Rev 80(3):545–563. 10.1128/MMBR.00005-16 [PubMed: 27250769]

Tartakoff A, DiMario P, Hurt E, McStay B, Panse VG, Tollervey D (2022) The dual nature of the nucleolus. Genes Dev 36(13–14):765–769. 10.1101/gad.349748.122 [PubMed: 36342833]

Thiry M, Goessens G (1992) Where, within the nucleolus, are the rRNA genes located? Exp Cell Res 200(1):1–4. 10.1016/s0014-4827(05)80064-3 [PubMed: 1563477]

van Sluis M, Gailín MÓ, McCarter JGW, Mangan H, Grob A, McStay B (2019) Human NORs, comprising rDNA arrays and functionally conserved distal elements, are located within dynamic

chromosomal regions. Genes Dev. 33(23–24):1688–1701. 10.1101/gad.331892.119 [PubMed: 31727772]

Vanden Broeck A, Klinge S (2022) An emerging mechanism for the maturation of the Small Subunit Processome. Curr Opin Struct Biol 73:102331. 10.1016/j.sbi.2022.102331 [PubMed: 35176592]

Vanden Broeck A, Klinge S (2023) Principles of human pre-60S biogenesis. Science. 381(6653):3892. 10.1126/science.adh3892

Wei T, Najmi SM, Liu H, Peltonen K, Kucerova A, Schneider DA, Laiho M (2018) Small-molecule targeting of RNA polymerase I activates a conserved transcription elongation checkpoint. Cell Rep 23(2):404–414. 10.1016/j.celrep.2018.03.066 [PubMed: 29642000]

White MR, Mitrea DM, Zhang P, Stanley CB, Cassidy DE, Nourse A, Phillips AH, Tolbert M, Taylor JP, Kriwacki RW (2019) C9orf72 Poly(PR) dipeptide repeats disturb biomolecular phase separation and disrupt nucleolar function. Mol Cell. 74(4):713–728.e6. 10.1016/j.molcel.2019.03.019 [PubMed: 30981631]

Xu H, Hurley LH (2022) A first-in-class clinical G-quadruplex-targeting drug. The bench-to-bedside translation of the fluoroquinolone QQ58 to CX-5461 (Pidnarulex). Bioorg Med Chem Lett. 77:129016. 10.1016/j.bmcl.2022.129016 [PubMed: 36195286]

Xu H, Di Antonio M, McKinney S, Mathew V, Ho B, O'Neil NJ, Santos ND, Silvester J, Wei V, Garcia J, Kabeer F, Lai D, Soriano P, Banáth J, Chiu DS, Yap D, Le DD, Ye FB, Zhang A, Thu K, Soong J, Lin SC, Tsai AH, Osako T, Algara T, Saunders DN, Wong J, Xian J, Bally MB, Brenton JD, Brown GW, Shah SP, Cescon D, Mak TW, Caldas C, Stirling PC, Hieter P, Balasubramanian S, Aparicio S (2017) CX-5461 is a DNA G-quadruplex stabilizer with selective lethality in BRCA1/2 deficient tumours. Nat Commun 8:14432. 10.1038/ncomms14432 [PubMed: 28211448]

Yamamoto T, Yamazaki T, Ninomiya K, Hirose T (2023) Nascent ribosomal RNA act as surfactant that suppresses growth of fibrillar centers in nucleolus. Commun Biol 6(1):1129. 10.1038/s42003-023-05519-1 [PubMed: 37935838]

Yang Y, Isaac C, Wang C, Dragon F, Pogacic V, Meier UT (2000) Conserved composition of mammalian box H/ACA and box C/D small nucleolar ribonucleoprotein particles and their interaction with the common factor Nopp140. Mol Biol Cell 11(2):567–577. 10.1091/mbc.11.2.567 [PubMed: 10679015]

Yao RW, Xu G, Wang Y, Shan L, Luan PF, Wang Y, Wu M, Yang LZ, Xing YH, Yang L, Chen LL (2019) Nascent pre-rRNA sorting via phase separation drives the assembly of dense fibrillar components in the human nucleolus. Mol Cell 76(5):767–783.e11. 10.1016/j.molcel.2019.08.014 [PubMed: 31540874]

Yap K, Mukhina S, Zhang G, Tan JSC, Ong HS, Makeyev EV (2018) A short tandem repeat-enriched RNA assembles a nuclear compartment to control alternative splicing and promote cell survival. Mol Cell. 72(3):525–540.e13. 10.1016/j.molcel.2018.08.041 [PubMed: 30318443]

Zisi A, Bartek J, Lindström MS (2022) Targeting ribosome biogenesis in cancer: lessons learned and way forward. Cancers (Basel) 14(9):2126. 10.3390/cancers14092126 [PubMed: 35565259]

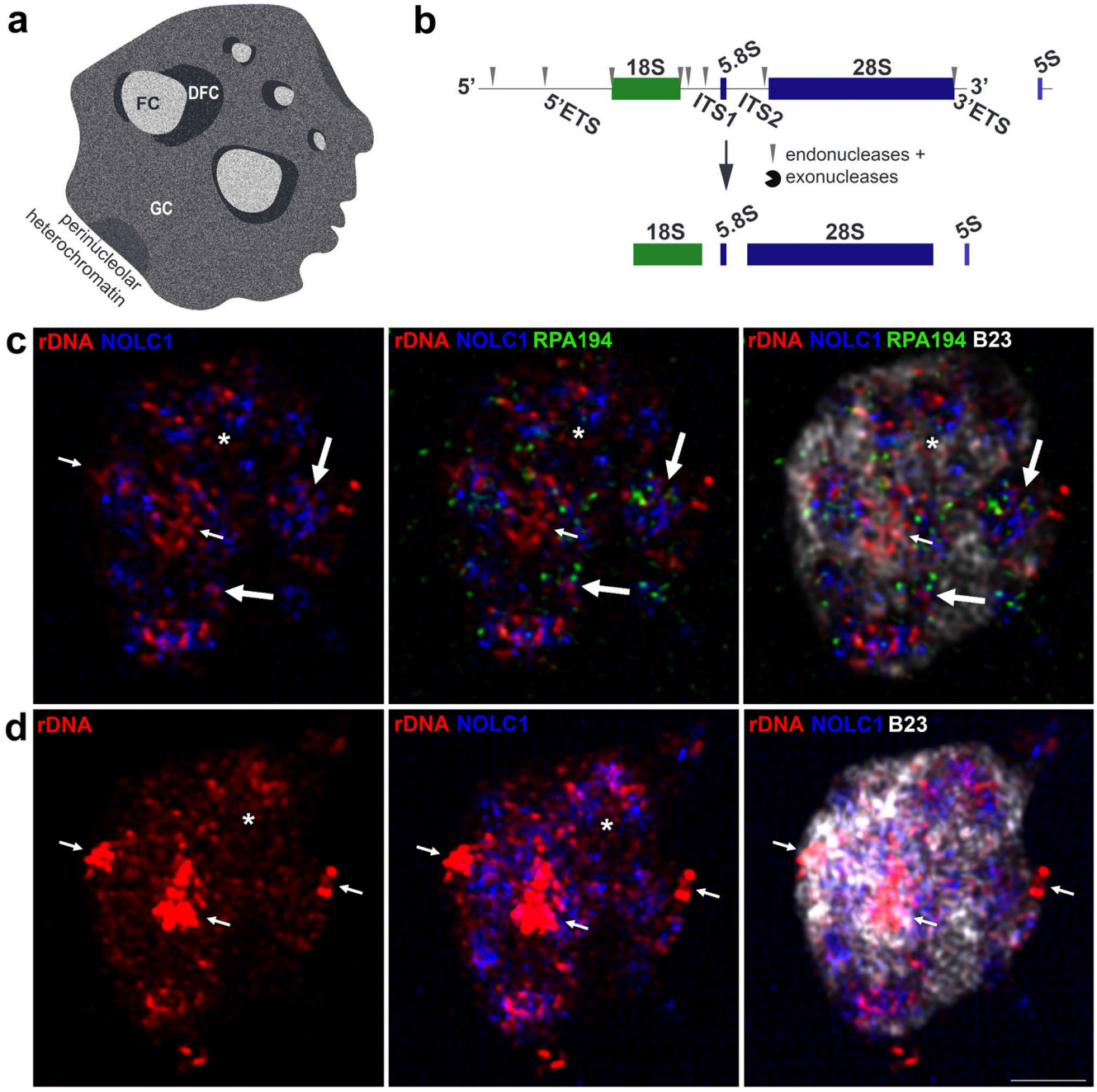

Fig. 1.

Functional suborganization of the nucleolus and visualization of the topology of ribosomal genes in the nucleolus. **a** Schematic representation of the three-layered structure of the nucleolus detected by negatively stained electron transmission microscopy. The pale, centrally positioned fibrillar center (FC) is surrounded by densely stained dense fibrillar component (DFC) and the outmost layer, granular component (GC), with numerous particles indicating the presence of preribosomal particles. **b** Schematic representation of the human precursor 47S rDNA gene array, which comprises the mature 18S, 5.8S, and 28S rRNA.

The external (5′ETS and 3′ETS) and internal (ITS1 and ITS2) transcribed spacers in the 47S primary transcript precursor are removed during step-wise pre-rRNA processing by individual cleavages targeted by endo- and exonucleases. The endonucleolytic cleavage sites are marked with arrowheads. **c, d** The topology of active, silenced, and constitutively inactive rDNA genes within the nucleolus of HeLa cells was detected by DNA FISH using three-dimensional (3D) SIM imaging. **c** Representative multicolor single-frame images. **d** Maximum intensity projection of five frames. The cell was hybridized with a DNA FISH probe against the rDNA coding sequence containing 5′ETS and 18S rRNA and codetected with the RNA pol I transcription machinery (RPA194), pre-rRNA processing (NOLC1), and preribosome assembly (B23/Nucleophosmin). The active rDNA genes detected with RPA194 and NOLC1 are in a linear relaxed pattern in active transcription/processing centers (large arrows). The silenced genes are visible in a relaxed pattern without marks of transcription/processing within the nucleolus (asterisks). In contrast, the constitutively inactive rDNA genes are located in the dense packs of heterochromatin situated at the periphery of the nucleolus (small arrows). Scale bars (**c** and **d**), 2 μm

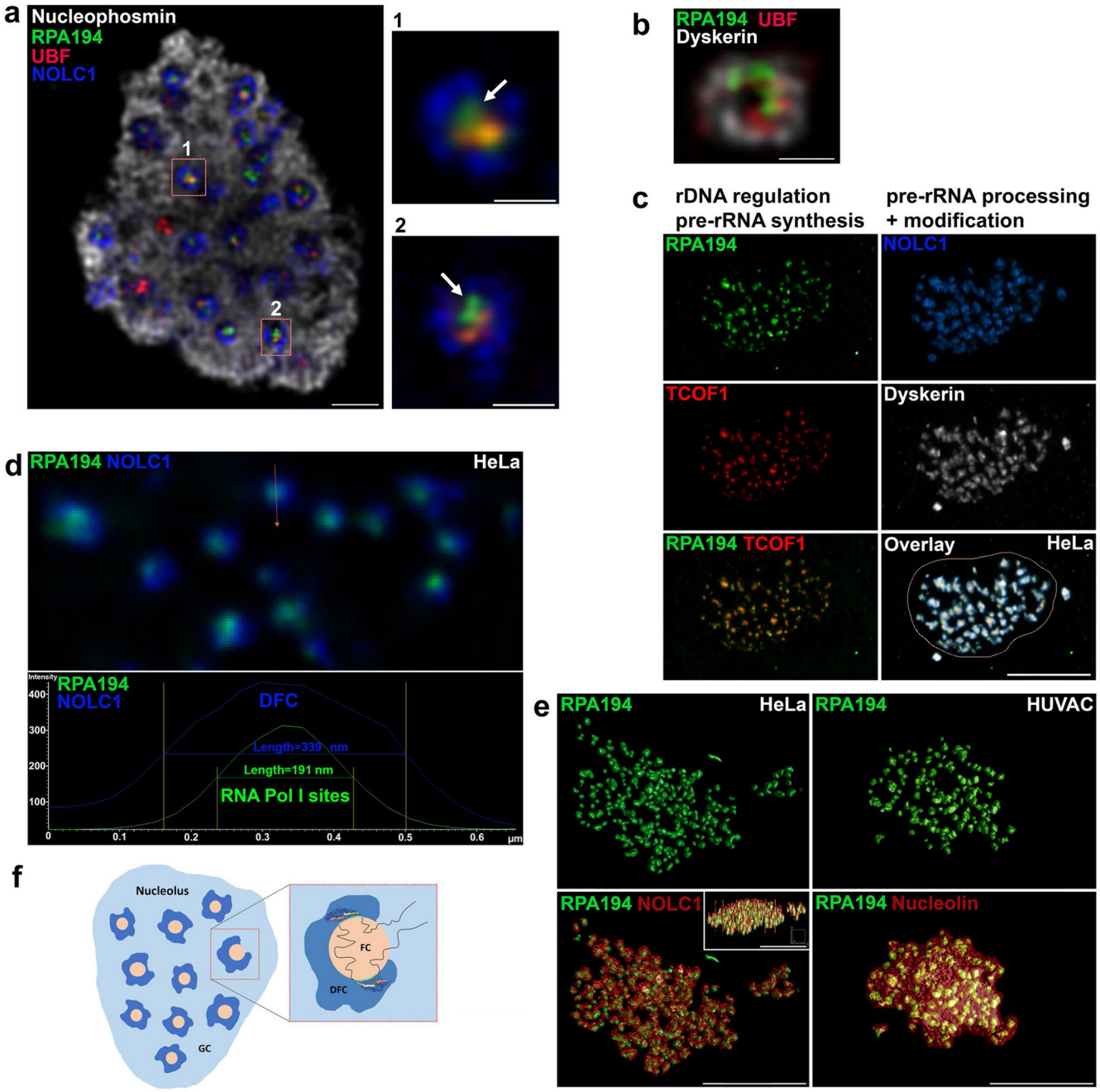

Fig. 2.

Functional characterization of FC/DFC units in the nucleolus. **a** Nucleolar overview with codetection of active RNA pol I complex (RPA194) with architectural chromatin factor UBF, pre-rRNA processing in DFC (NOLC1) and GC region assembly chaperone nucleophosmin using SIM imaging in HeLa cells. Representative prominent nucleolus in HeLa cells contains numerous small FC/DFC units localized in evenly distributed arrangements (left). Two magnified regions (indicated in the entire nucleolus by two dashed boxes marked as 1 and 2, left) demonstrate that FC/DFC units are organized as small ring-shaped structures

with UBF localized in the core of FC and active rDNA transcription site(s) (RPA194) protrudes from the periphery of FC into the DFC interior marked with Dyskerin or NOLC1 (right, arrows). **b** The image of the magnified FC/DFC unit demonstrates the internally positioned UBF with pre-rRNA synthesis marked with RPA194 toward DFC detected by Dyskerin, a pre-rRNA base modification enzyme. **c** Nucleolar codetection of four individual marker components of FCs (RPA194 and TCOF1) and DFC (NOLC1 and Dyskerin) using the multichannel 3D detection in the active nucleolus in HeLa cell using Nikon AXR NSPARC 3D super-resolution microscopy. The 3D topology of FC/DFC units, which was detected within the entire nucleolar volume, demonstrates that all RNA pol I transcription sites (RPA194, TCOF1) codetect with pre-rRNA processing/modification factors (NOLC1 and Dyskerin) as uniform functional units. **d** Measurement of the diameter length (marked with red arrow) of 3D visualization of active RNA pol I transcription site and surrounding DFC in HeLa cells. The upper image is a 3D visualization, with a single FC/DFC measured below. **e** Quantitation of FC/DFC units by codetection of RP194 transcription site, NOLC1 and Nucleolin (histone chaperone required for rRNA metabolism), in aneuploid HeLa cells and diploid HUVAC cells, visualized by 3D volume rendering using 3D SIM images. The inset in the lower left panel shows the orthogonal view of the nucleolus. **f** The schematic representation highlights the presence of numerous small FC/DFC units scattered throughout the whole nucleolus (left, box). The enlarged structural organization of one FC/DFC unit with two transcriptionally active rDNA genes at the FC/DFC boundary is shown on the right. Scale bars, (**a**, left) 1 μm; (**a**, right and **b**, 500 nm). Scale bars (**c** and **e**) 5 μm

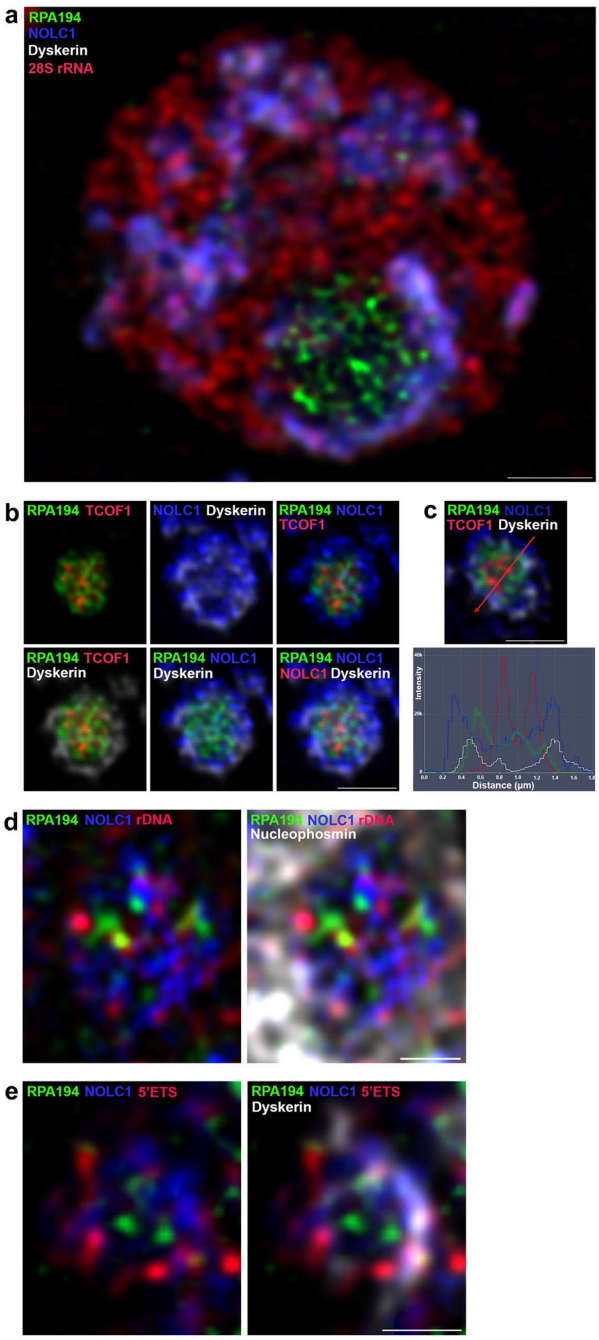

Fig. 3.

Substructural organization of highly enlarged FCs in the nucleolus using SIM imaging. **a** Nucleoli in HeLa cells with enlarged FCs contain higher numbers of fiber-like RNA pol I transcription sites (RPA194) within the FC interior and are surrounded by larger DFC (detected by NOLC1 and Dyskerin) and 28S rRNA by RNA FISH, present in DFC and GC. **b** Suborganization of the larger FC/DFC units. The architectural FC protein TCOF1 is located in the inner core of the FCs, and active RNA pol I sites protrude toward DFC. NOLC1, which interacts with RNA pol I, is also present in the FC but mainly in the DFC.

Detection with Dyskerin indicated that modifications of pre-rRNA bases occur in the DFC. **c** A line-scan profile across the large FC/DFC in HeLa cell shows centrally positioned TCOF1, active RNA pol I (RPA194) in outer FC and FC/DFC boundary and NOLC1 present across the FC and prominently in the DFC. Pseudouridinylation of pre-rRNA by Dyskerin likely occurs in the inner DFC region. **d** Large FCs harbor an increased number of internally located rDNA genes than small FC/DFC modules demonstrated by rDNA FISH. **e** Localization of the nascent pre-rRNA synthesis and processing by RNA FISH revealed that the cotranscriptionally processed 5′ETS leader upstream of the first cleavage site is rapidly relocalized from the periphery of the FC to DFC. Scale bars, (*a*, **b**) 1 μm; (**d**, **e**) 500 nm

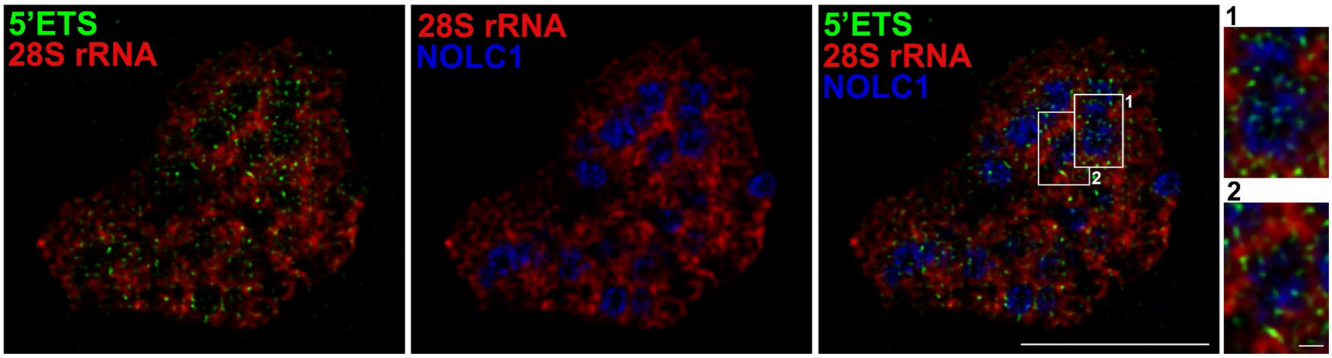

Fig. 4.

Spatial distribution of pre-rRNA processing segments in the nucleolus. Simultaneous two-color RNA FISH hybridizing the 5′ETS leader sequence and 28S rRNAs along with detection of NOLC1 as a marker for the DFC. Individual images demonstrate combinatorial codetection of the unstable 5′ETS leader sequence with 28S rRNA. Mature 28S rRNAs are detected in DFC as a part of the nascent primary transcript but dominantly accumulated in GC. Two magnified regions (indicated in the overlay image of the entire nucleolus by two boxes marked as 1 and 2, left) demonstrates active transcription sites where the 5'ETS FISH signals are codetected with 28S rRNA in FC/DFC units detected with NOLC1. Scale bars, 4 μm, 500 nm (right)

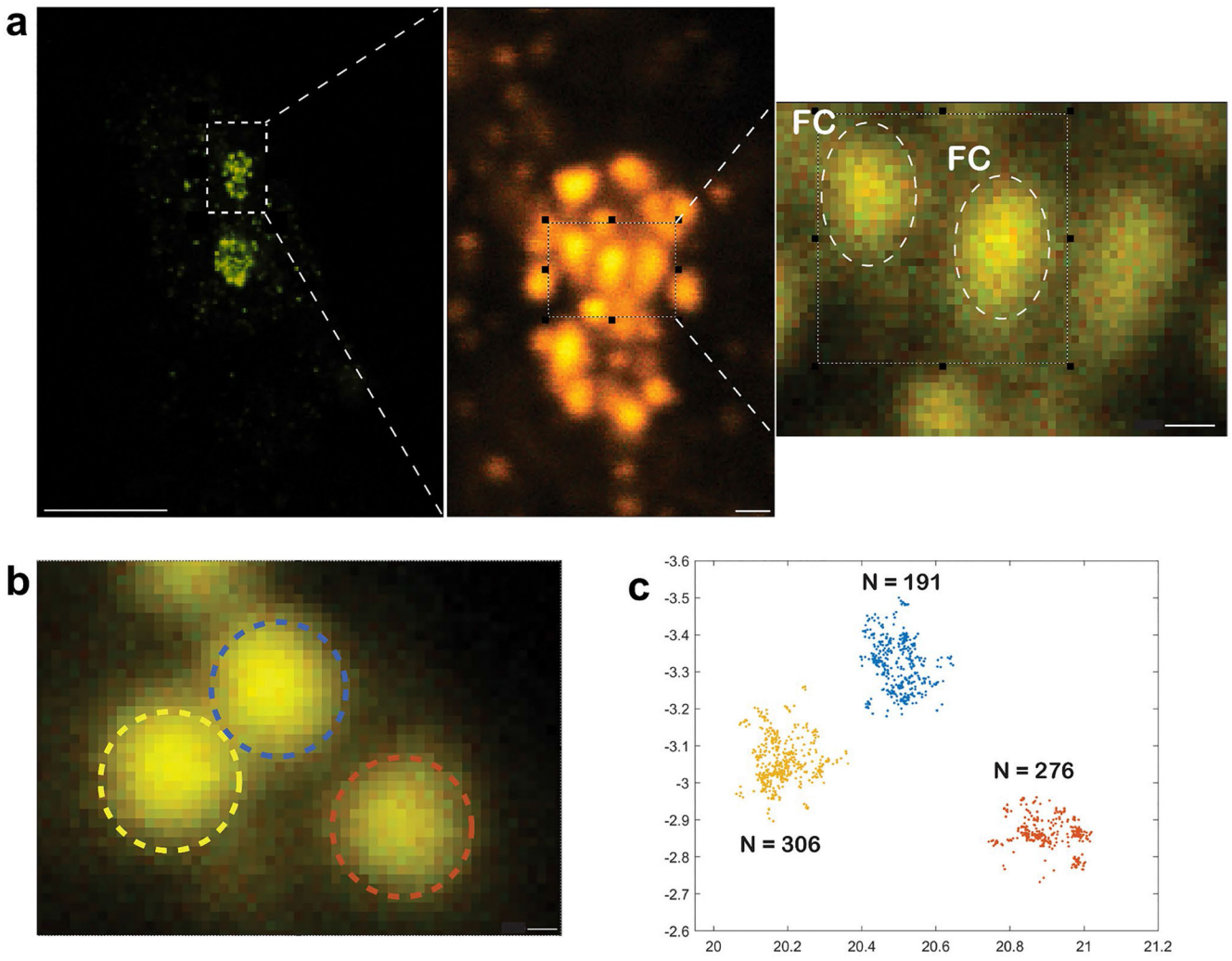

Fig. 5.

Functional suborganization of RNA pol I transcription complexes at single molecule levels by MINFLUX nanoscopy. **a** Localization of RPA194 in small FCs in HeLa cells by confocal microscopy at increasing magnification from left to right. Two prominent FCs are highlighted in the nucleolus (right). **b** The image with three prominent small FCs (highlighted in the yellow, blue, and red ovals) was subjected to recording individual positions of RPA194 molecules using MINFLUX nanoscopy (**c**). The resulting data were processed to ensure each localized RPA194 signal represented an individual protein. The numbers of detected RPA194 molecules in three designated individual FCs are shown on the plot in corresponding colors (right). Analysis revealed that one small FC contains an average of 212.5 ± 30.1 individual RPA194 molecules, which is in agreement with our observations that one small FC/DFC forms on one or two active rDNA genes. Scale bars (**a**, from left to right), 10 μm, 500 nm, and 200 nm; (**b**) 100 nm

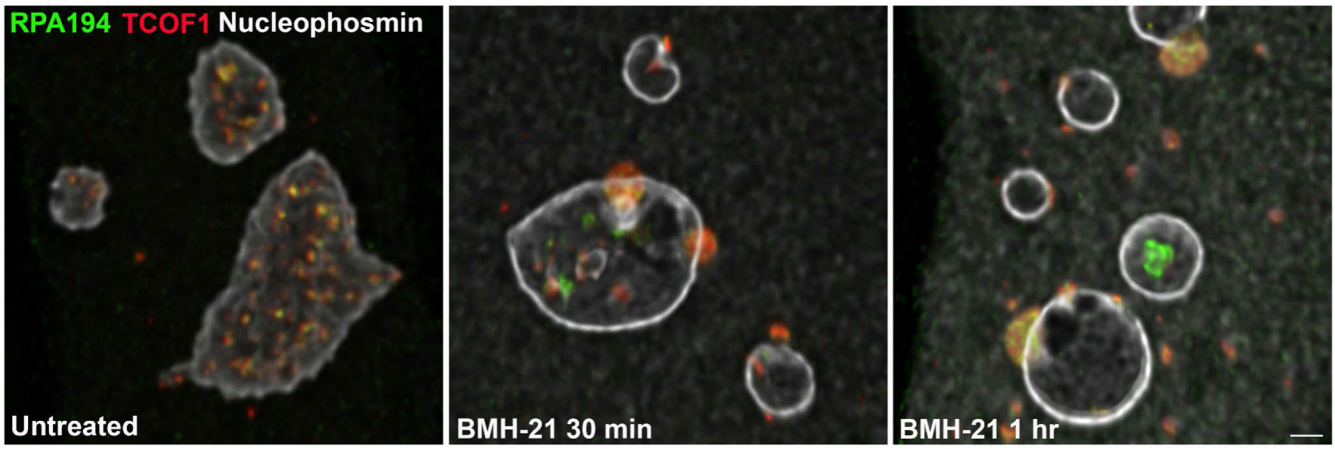

Fig. 6.

The effect of RNA pol I inhibitor BMH-21 on the structural architecture of the nucleolus. Nikon NSPARC 3D microscopy demonstrating the short inhibition of pre-rRNA synthesis by BMH-21, the nucleoli gradually lose their irregularity, rough outer edges of GC become roundish with a liquid-like appearance, and RNA pol I transcription sites coalesce, form prominent nucleolar caps at the nucleolar periphery and segregate from other nucleolar layers upon treatment with BMH-21 due to lack of ongoing pre-rRNA synthesis. Scale bar, 1 μm

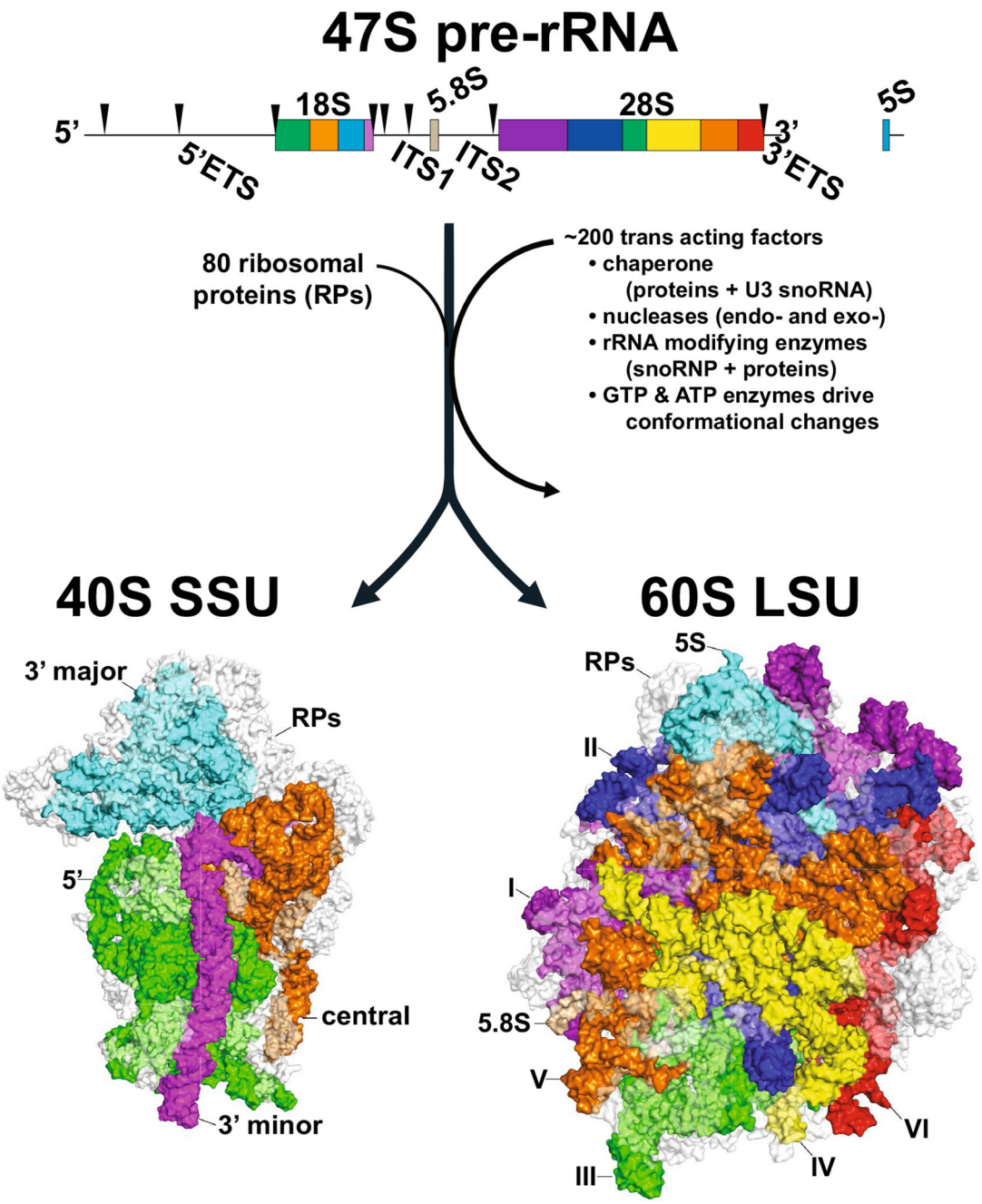

Fig. 7.

Overview of human ribosome biogenesis. At the top is the schematic for the 47S pre-rRNA pol I transcript with the external and internal spacer elements (5′ETS, ITS1, ITS2, and 3′ETS) flanking the four domains of 18S (green, orange, cyan, and magenta), 5.8S, and the six subdomains of the 28S (purple, blue, green, yellow, orange, and red). Each endonucleolytic cleavage is shown as a black arrowhead with the second and third ones from the left shown in more detail as A0 and A1 in Fig. 8. RNA pol III transcribes 5S from a separate gene. Below on the left is the cryo EM structure of the mature 40S small

ribosomal subunit (SSU) showing the four distinct domains [The Protein Data Bank (PDB) 6G5H]. Below, on the right, is the cryo EM structure of the mature 60S large ribosomal subunit (LSU) showing how the six subdomains interdigitate to form one massive domain PDB (8A3D). A white transparent surface represents the RPs of both structures

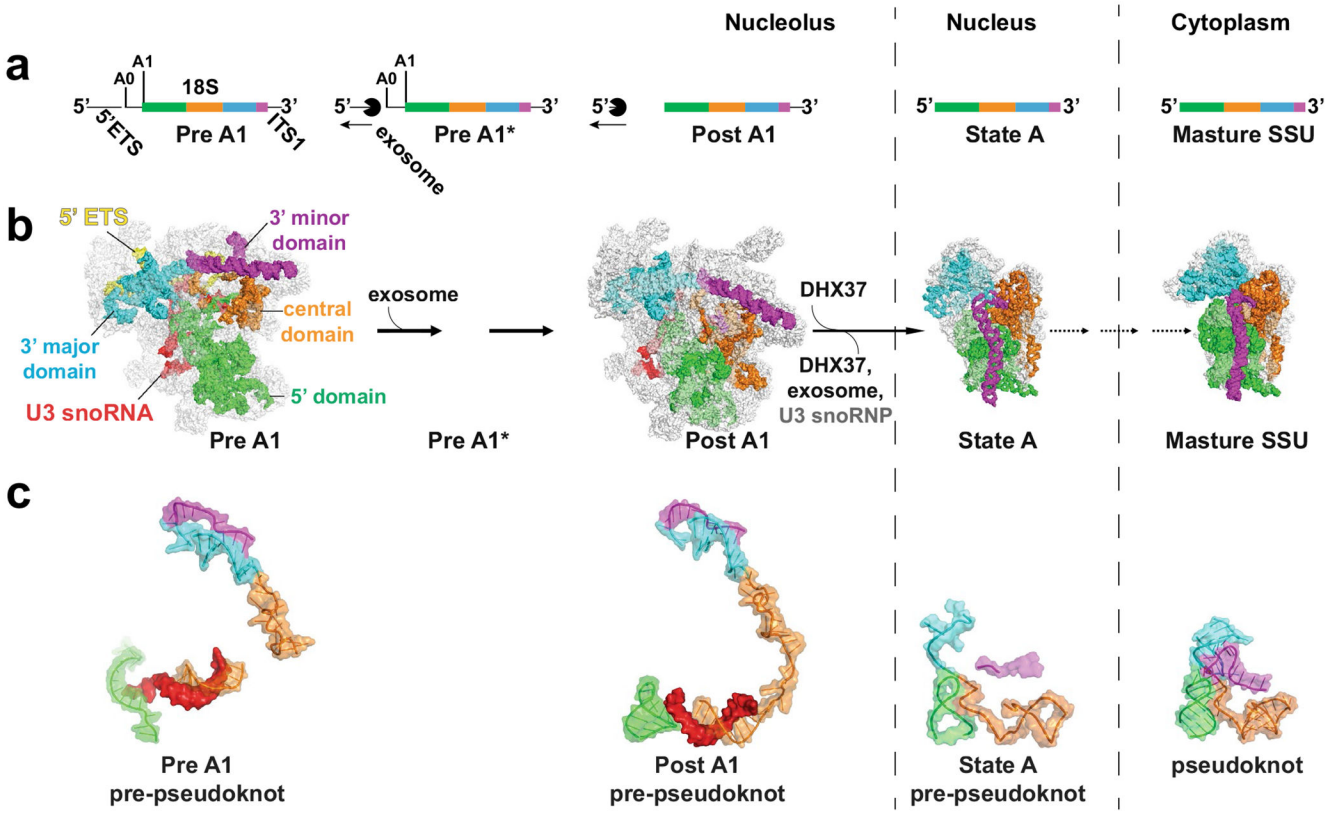

Fig. 8.

Overview of SSU biogenesis in the nucleolus, nucleus, and cytoplasm. **a** The SSU part of pre-rRNA, which includes the 5′ETS, 18S (all four subunits from 5′ to 3′ green, orange, cyan, and magenta), and ITS1. From human cells, three cryoEM intermediates have been observed that occur in the nucleolus. Pre-A1 is after cleavage at A0 but before cleavage at A1. Pre-A1* is after exosome begins 3′→ 5′ exonuclease activity but before A1 cleavage. Post-A1 is after both cleavage events. State A is the first nuclear intermediate observed for human cells in the nucleus. **b** CryoEM structures of pre-A1, post-A1, state A, and the mature SSU (PDB entries 7MQ8, 7MQA, 6G4W, and 6G5H, respectively). rRNA domains are color coded as in **a**, and all proteins appears as white transparent surfaces. **c** Zoom-in on the folding of the universally conserved central pseudoknot from the pre-A1, the post-A1, the state A, and the mature SSU

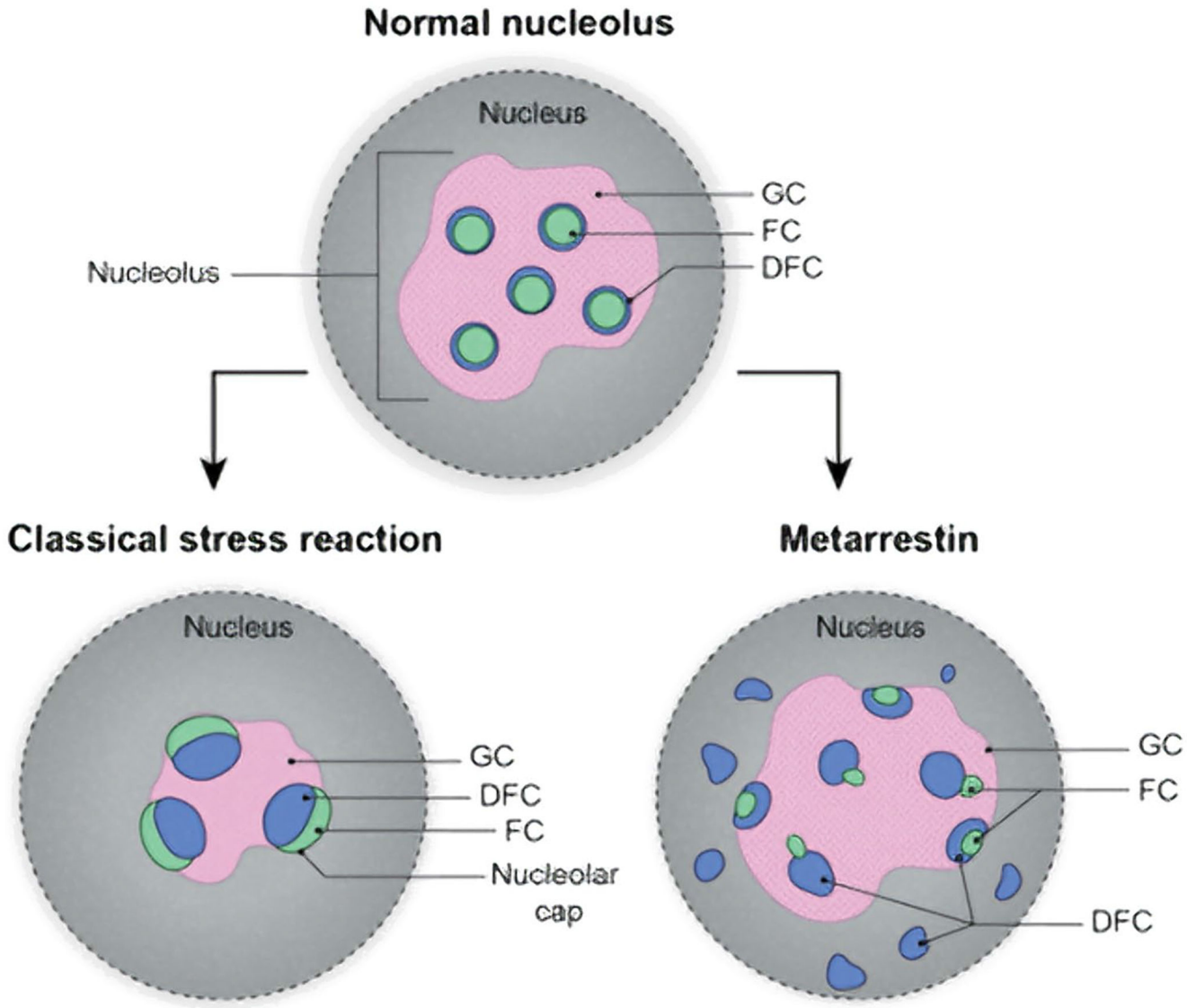

Fig. 9.

Nucleolar stress induced by anti-cancer drugs is associated with unique ultrastructural changes governed by underlying mechanism of administered agents. Illustration of classical nucleolar cap formation associated with decreased nucleolar volume and rounding of the nucleolus by genotoxic agents, such as actinomycin D and CX-5461, on left versus loss of phase partitions due to lowering of LPPS leading to increase of smaller DFC units after oxaliplatin or metarrestin treatment

Table 1

Inhibitors of rDNA transcription

Name	Selective for nucleolar function	Genotoxicity	RiBi checkpoint activation	Mechanism	Clinical development	Outcome	NCT no.
Oxaliplatin	No	Yes	Yes	FBL-mediated loss of nucleolar phase separation between DFC and GC components	Approved standard-of-care for colon cancer; off-label use for several GI cancers, often in combination with 5-FU		
CX-3543	Yes	No	Yes	Disrupt nucleolin/rDNA G-quadruplex complexes	Phase I	Terminated due to poor biodistribution	NCT00955786; NCT00955292; NCT00780663
CX5461	No	Yes	Yes	intercalation and stabilization of G-quadruplexes leading to halt of replication, genomic instability, and DNA breaks	Phase I (CCTG IND.231)	Preliminary clinical effiacy to determine chronic tolerable and recommended phase II dose level; further safety evaluation in expansion phase IB	NCT02719977; NCT04890613
BMH-21	Yes	No	Yes	Intercalation into GC-rich rDNA regions, inhibition of polymerase I elongation, and proteosomal degradation of RP-194	Preclinical	Not selected for clinical development due to off-target effects	
Metarrestin	Yes	No	No	Disassembly of the perinucleolar compartment (PNC), a marker of nuclear genome organization for cancer metastasis	Phase I		NCT04222413

Histochem Cell Biol. Author manuscript; available in PMC 2024 August 18.